Published in final edited form as:

Cell Rep. 2019 January 15; 26(3): 702–719.e6. doi:10.1016/j.celrep.2018.12.080.

Rbf Activates the Myogenic Transcriptional Program to Promote Skeletal Muscle Differentiation

Maria Paula Zappia[1], **Alice Rogers**[1], **Abul B.M.M.K. Islam**[2], and **Maxim V. Frolov**[1,3,*]

[1]Department of Biochemistry and Molecular Genetics, University of Illinois at Chicago, 900 S. Ashland Avenue, Chicago, IL 60607, USA

[2]Department of Genetic Engineering and Biotechnology, University of Dhaka, Dhaka 1000, Bangladesh

[3]Lead Contact

SUMMARY

The importance of the retinoblastoma tumor suppressor protein pRB in cell cycle control is well established. However, less is known about its role in differentiation during animal development. Here, we investigated the role of Rbf, the *Drosophila* pRB homolog, in adult skeletal muscles. We found that the depletion of Rbf severely reduced muscle growth and altered myofibrillogenesis but only minimally affected myoblast proliferation. We identified an Rbf-dependent transcriptional program in late muscle development that is distinct from the canonical role of Rbf in cell cycle control. Unexpectedly, Rbf acts as a transcriptional activator of the myogenic and metabolic genes in the growing muscles. The genomic regions bound by Rbf contained the binding sites of several factors that genetically interacted with Rbf by modulating Rbf-dependent phenotype. Thus, our results reveal a distinctive role for Rbf as a direct activator of the myogenic transcriptional program that drives late muscle differentiation.

Graphical Abstract

*Correspondence: mfrolov@uic.edu.

AUTHOR CONTRIBUTIONS

M.P.Z. and M.V.F. conceived the project, designed the experiments, analyzed data, and wrote the manuscript. M.P.Z. performed most of the experiments with important support from A.R., who generated all data related to the Dmd8 cells and the knockdown with *Act88F* driver. A.B.M.M.K.I. performed the bioinformatics data analysis of high-throughput sequencing data sets. All authors reviewed and edited the manuscript

SUPPLEMENTAL INFORMATION

Supplemental Information includes two figures and seven tables and can be found with this article online at https://doi.org/10.1016/j.celrep.2018.12.080.

DECLARATION OF INTERESTS

The authors declare no competing interests.

SUPPORTING CITATIONS

The following reference appears in the Supplemental Information: Anders and Huber (2010).

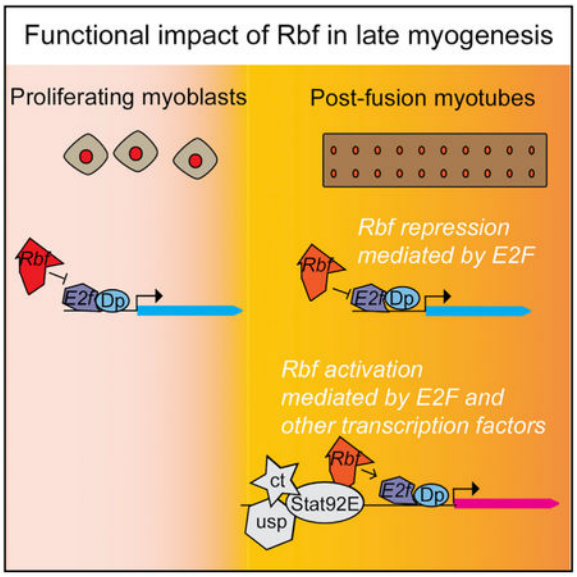

In Brief

Inactivation of the tumor suppressor RB, an obligatory step in most cancers, results in unrestrained cell cycle progression. Zappia et al. show that Rbf, the RB *Drosophila* ortholog, directly activates the metabolic program that accompanies muscle development. This work expands the understanding of the plethora of Rbf functions.

INTRODUCTION

The retinoblastoma (pRB) tumor suppressor protein is a multifunctional protein that is best known for its role in controlling cell cycle because it inhibits the E2F transcription factor. The functional inactivation of pRB is considered to be an obligatory event in human cancer and underscores the importance of pRB in tumorigenesis. However, whether the ability of pRB to promote cell cycle exit entirely accounts for its tumor suppressive property remains an unresolved question. This is mostly because the inactivation of pRB also reduces cell differentiation, including lipogenesis (Classon et al., 2000), myogenesis (de Bruin et al., 2003; Zacksenhaus et al., 1996), erythropoiesis (Spike et al., 2004), and osteogenesis (Thomas et al., 2001). However, deciphering the actual role of pRB in differentiation *in vivo* is complicated because the inactivation of RB often leads to ectopic cell proliferation and apoptosis, which may account for the differentiation defects. Thus, it is important to identify the *in vivo* settings where the bona fide role of pRB in differentiation can be investigated without the accompanied ectopic cell cycles.

The model organisms, such as *Drosophila*, are advantageous in providing insights into gene function during development. Mammals and flies share significant similarity in the arrangement of the E2F/pRB pathway, whereas the *Drosophila* E2F and pRB families are smaller. Therefore, redundancy and compensation among family members is attenuated. E2F is a heterodimer between an E2F subunit and a DP subunit. In *Drosophila*, there are two E2F genes, *E2f1* and *E2f2*, a single gene encoding a DP subunit, and two pRB-related genes, *Rbf*

and *Rbf2*. Either E2F1 or E2f2 requires Dp to bind to DNA. Therefore, the loss of Dp inactivates both E2Fs. In general, E2f1 is an activator of gene expression and is negatively regulated by Rbf, whereas the repressor E2f2 forms a repressive complex with either Rbf or Rbf2 (dREAM/Myb-MuvB). Unlike Rbf, the expression of Rbf2 is restricted to a few cell types, and it appears to be less significant than Rbf at late stages of development. The phenotype of *Rbf* mutants is highly reminiscent of the inactivation of RB in mammals and results in increased apoptosis and abnormal cell cycles (Du and Dyson, 1999). Genome-wide studies revealed that Rbf binds to chromatin in an E2F-dependent manner (Korenjak et al., 2012) and can either limit E2f1 activation or repress tissue-specific transcriptional programs in conjunction with E2f2 (Dimova et al., 2003; Lewis et al., 2004). Thus, Rbf is widely considered to be a transcriptional repressor.

Surprisingly, the loss of both E2Fs is permissive for most *Drosophila* development, and the patterns of cell proliferation and differentiation are largely normal. However, E2F is essential for animal viability because E2F-deficient animals die at the pupal stage because of severe defects in adult skeletal muscles (Zappia and Frolov, 2016) and in the fat body (Guarner et al., 2017). In skeletal muscles, E2F is needed for full activation of myogenic genes during muscle growth and myofibrillogenesis. E2f1 occupies the promoter region of several myogenic genes and directly regulates their expression. Interestingly, in addition to E2f1, Rbf occupancy is also enriched at the same genes. Because Rbf is a known inhibitor of E2f1, one could reason that Rbf may limit the activation of the myogenic E2F target genes and subsequently affect muscle development. However, the role of Rbf in myogenesis has not been studied.

Here, we investigated how the inactivation of Rbf affects the development of the adult skeletal muscles. Unexpectedly, we found that Rbf functions as an activator of the myogenic transcriptional program. The depletion of Rbf during myogenesis phenocopies the loss of E2F, i.e., severe reduction in muscle size, abnormal myofibrillogenesis, and incomplete activation of the myogenic genes. Importantly, the differentiation defects of Rbf-depleted muscles occur without concomitant ectopic cell cycles. Computational analysis identified putative binding sites of ultraspiracle (usp), cut (ct), and signal-transducer and activator of transcription protein at 92E (Stat92E) in the promoters of the myogenic Rbf targets. The genetic-interaction experiments revealed that Rbf and these factors act synergistically. Thus, Rbf has a direct role in the differentiation during muscle development.

RESULTS

The Effect of Rbf Function in a Cell Culture-Based Model of Myogenic Differentiation Is Conserved between *Drosophila* and Mammals

Important insights into the role of the mammalian pRB were obtained using an *in vitro* myogenic differentiation model. Thus, we established a similar cell culture-based model using *Drosophila*. The Dmd8 cell line is derived from myoblasts of the wings discs of third instar larvae (Ui et al., 1987). We optimized the culturing conditions to robustly induce differentiation of Dmd8 myoblasts into multinucleated myotubes (see STAR Methods). The addition of the differentiation medium resulted in distinct morphological changes over time. This process was accompanied by a robust induction of the master myogenic transcription

factor Myocyte enhancer factor 2 (Mef2; Figure 1A). At 6 days, the number of nuclei per cell was markedly increased, and some cells became highly elongated and resembled myotubes (Figure 1B).

To confirm that the observed morphological changes reflect the progression of myogenesis, we monitored the expression of several key myogenic genes that are routinely used as markers *in vivo*. Differentiation of myoblasts into adult skeletal muscles is accompanied by the upregulation of *Mef2* with concomitant downregulation of *twist* (*twi*), *heartless* (*htl*), and *stumps*. We examined the expression of these genes at 0, 3, 6, and 9 days after the addition of differentiation medium to Dmd8 cells. Notably, these genes were downregulated through day 9 (Figure 1C, top). The expression of genes encoding for structural proteins, such as *flightin, Myosin light chain2*, and *Tropomyosin1*, were induced and increased over time (*fln, Mlc2,* and *Tm1*, respectively; Figure 1C, bottom). Overall, our data suggest that the myogenic transcriptional program is properly induced in the Dmd8 cell culture-based model and that the observed morphological changes indeed reflect the formation of myotubes and, in particular, fairly replicate the early phase of the indirect flight muscle development.

Having established the robust protocol of *in vitro* myogenic differentiation using Dmd8 cells, we set to probe the role of Rbf in this system. Dmd8 cells were incubated with *Rbf*-double-stranded RNA (dsRNA) to deplete the expression of Rbf by RNAi, and *GFP*-dsRNA was used as control. The efficiency of Rbf depletion, confirmed by western blot (Figure 1D), had almost no effect on cell proliferation at day 0 as revealed by anti-PhosphorHistone H3 (pH3) staining that marks mitotic cells (Figure 1E). In addition, the analyses at days 3 and 6, upon differentiation, indicated that Rbf-depleted cells exit the cell cycle on time (Figure 1E). However, Rbf-depleted cells were partially impaired in their ability to undergo myogenic differentiation (Figure 1F). The number of nuclei within syncytial myotube was slightly reduced compared with the control (Figure 1F, right). The depletion of Rbf was confirmed by measuring the expression of *Rbf* at the end of the experiment on day 6 (Figure 1G). Thus, the loss of Rbf in cultured Dmd8 myoblasts partially affects the ability of cells to form multinucleated myotubes but does not affect the cell cycle exit.

The Loss of Rbf Affects the Proliferation of the Adult Muscle Precursors *In Vivo*

The observation that the depletion of Rbf impairs myotube formation *in vitro* was intriguing. Thus, we investigated Rbf function in a more relevant *in vivo* system, such as the developing adult skeletal muscles in *Drosophila*. We focused on the indirect flight muscles (IFMs) because they most resemble mammalian skeletal muscles, and their development is described in great detail. There are two types of IFMs: the dorsal-longitudinal muscles (DLMs) and the dorsoventral muscles (DVMs). DLMs are formed by remodeling larval muscles that serve as templates to which myoblasts fuse, whereas DVMs are formed *de novo* by myoblast fusion (Dutta et al., 2004; Fernandes et al., 1991). The myoblasts that give rise to the IFMs are specified earlier during embryogenesis and are located in the adepithelial layer of the wing discs. Myoblasts can be marked with the *twi-lacZ* transgene that is expressed continuously in these cells until they fuse to form myotubes. Dividing myoblasts were visualized by immunofluorescence using the pH3 antibody. In the wild type, myoblasts actively proliferate during larval and early pupal stages as they migrate to fuse with

developing DLMs (Figure 2A). Around 16 h after pupa formation (APF), the three larval templates split, which results in six myotubes that initiate their compaction and attachment to tendons. Between 24 and 29 h APF, the number of unfused myoblasts (*twi-lacZ* positive), and consequently, pH3-positive cells, drop significantly. By 33 h APF, the fusion is complete, and no remaining myoblasts are detected (Figure 2A and 2B). Upon completion of fusion, myofibers are thickening and shortening. Then, from mid to late pupa muscles elongate and fill the entire adult thorax.

Such strict order of events during the development of IFMs allowed us to determine precisely the effect of Rbf depletion in muscle differentiation. The early larval lethality of the Rbf mutants precludes such analysis. Therefore, we used RNAi to deplete Rbf specifically in muscles by driving *UAS-Rbf-RNAi* with the muscle-specific *Mef2-GAL4* driver. To confirm the efficiency of Rbf depletion, wing discs of third instar larvae were stained with Rbf antibody and counterstained with Mef2 antibody to label myoblasts. As shown in Figure 2C, Rbf was specifically depleted in myoblasts but not in the adjacent epithelial cells of the wing discs. Notably, the depletion of Rbf with *Mef2-GAL4* resulted in fully penetrant pupal lethality, in which most animals died as pharate adults. We confirmed this phenotype with another muscle-specific GAL4 driver how^{24B}.

To assess the effect of Rbf depletion on myoblast proliferation, the number of mitotic myoblasts, labeled with pH3 antibody, was quantified at two time points: wing discs and 21 h APF. The number of pH3-positive myoblasts was slightly increased upon Rbf depletion compared with control wing discs (Figure 2D). However, the total number of myoblasts was not significantly affected, indicating that Rbf-depleted myoblasts likely have more-extended mitosis than wild-type cells have. Developing DLMs at 21 h APF were labeled with the antibody 22C10 (Figure 2E). Similarly, the loss of Rbf resulted in an elevated number of myoblasts undergoing mitoses (Figure 2H). However, the timing of the cell cycle exit was not significantly affected because the number of pH3-positive cells dropped dramatically at 29 h APF, which is similar to that of control animals, and was mostly undetectable at 33 h APF (Figures 2F–2H). Thus, the depletion of Rbf results in an increase in the number of proliferating myoblasts but does not delay cell cycle exit during the formation of the indirect flight muscles.

Because Rbf-depleted myoblasts showed an increased mitotic index at 21 h APF, we asked whether some of these cells were eliminated by apoptosis. Developing DLMs were stained with antibodies against the death caspase-1 (Dcp-1), a critical executioner of apoptosis, throughout muscle development (21, 24, 29, 33, 43, 72, and 96 h APF; Figure S1). No Dcp-1 staining was detected in Rbf-depleted muscles or in the control, suggesting that the loss of Rbf does not appear to induce a detectable level of apoptosis in myoblasts. However, other apoptotic or nonapoptotic mechanisms, independent of Dcp-1, may be activated by the loss of Rbf.

Rbf Regulates Myofibril Formation and Muscle Growth

During myofibrillogenesis, the developing myotubes are gradually converted into myofiber by forming myofibrils and assembling presarcomeric structures, which dynamically mature into highly ordered repetitive contractile units, known as sarcomeres, as muscles grow and

elongate (Fernandes et al., 1991; Reedy and Beall, 1993). A mild defect was already evident upon Rbf depletion at the onset of myofibrillogenesis (Figures 2F and 2G). DLMs at 29 and 33 h APF were dissected and stained with phalloidin to visualize myofibril formation. Premyofibrils structure assembles first at the myofiber surface and then spread throughout the interior of the fiber (Sparrow and Schock, 2009). Although the surface of developing muscles showed proper formation of myofibrils, the interior plane of DLMs, taken 4 μm below the fiber surface, lacked the repetitive myofibril organization, and some myofibrils were missing (Figures 3A and 3B). In addition, the presarcomeric structures, which had an orderly display in control myofibrils, were abnormally organized in Rbf-depleted muscles. The precise process of assembling a highly regular array of myofibrils and sarcomere depends on the mechanical tension mediated by muscle attachment (Weitkunat et al., 2014). Because assembly was abnormal in Rbf-depleted muscle fiber, we examined the compaction of the fiber by measuring the length of muscle fibers at 29 h APF. Consistent with the observed defects, Rbf-depleted fibers were significantly longer than those of the control, implying a defect in tension (Figure 3C).

Given that *Mef2>Rbf-RNAi* animals die as pharate adults, we examined the formation of adult muscle at late pupa development (96 h APF) before the lethal stage. Persistence of Rbf knockdown at this developmental stage was confirmed by western blot (Figure 3D). The overall structure of IFM was analyzed by staining both transverse and sagittal cross-sections of thoraces. Notably, we found a severe reduction in muscle size in Rbf-depleted muscles, indicating defective muscle growth (Figure 3E). Additionally, myofibrils were not properly aligned and showed signs of actin clumps and defrayed phenotype (Figure 3F). This indicates that Rbf knockdown affects the proper regulation of muscle growth, as well as myofibrillogenesis, which is likely independent of its role in cell cycle control.

To further characterize the effect of Rbf depletion, we extracted RNA from IFMs and measured the expression of several known muscle-related genes (Figure 3G). In agreement with the phenotype described, the expression of genes encoding for components of sarcomeric structure and myofibrils, such as *fln, sarcomere length short* (*sals*), *Tropomyosin2* (*Tm2*), *Myosin heavy chain (Mhc), Actin88F (Act88F),* and *Mlc2*, were significantly reduced, along with the myogenic regulators *held out wings (how), Mef2,* and *spalt major (salm)*.

Because Rbf-depleted myoblasts showed an increased mitotic index at 21 h APF, we asked whether these extra myoblasts were fusing to the developing myotubes. We stained dissected muscles with DAPI and quantified the total number of nuclei per cross section of mature DLM. Notably, the number of nuclei was not significantly changed in Rbf-depleted muscles. Thus, despite an increase in pH3-positive myoblasts at the early stages of myogenesis (Figures 2D, 2E, and 2H), there is no significant effect on the total number of fused nuclei. Thus, our data indicate that either Rbf-depleted myoblasts take longer to complete mitosis or the extra myoblasts are eliminated by an alternative mechanism that is not mediated by Dcp1.

Overall, our data suggest that Rbf has an important role in skeletal-muscle development and that the loss of Rbf affects muscle growth and myofibrillogenesis, which is likely caused by reduced expression of the muscle-specific genes.

Rbf Activates the Myogenic Transcriptional Program during Muscle Development

As described above, the loss of Rbf in muscle results in two distinct phenotypes. First, there is increased proliferation in Rbf-depleted myoblasts before their fusion to myotubes. This phenotype reflects the well-known canonical function of Rbf as a negative regulator of cell proliferation. Then, in late developing DLM, the loss of Rbf impairs muscle growth and myofibrillogenesis. Thus, Rbf seems to be a positive regulator of myogenesis during late muscle differentiation. To investigate this function of Rbf, we identified the Rbf-dependent transcriptional program during muscle development.

We compared the wild-type transcriptomes between two developmental stages: proliferating myoblasts in wing discs and fully developed muscles in pharate adults (Figure 4A; Table S1). To enrich for the myoblast cell population, third-instar larval wing discs were dissected, and the notum, which contains myoblasts, was cut and used to isolate RNA. We note that the sample also contained wing disc epithelial cells that may mask the expression of myoblast-specific genes. In total, we have identified, by RNA sequencing (RNA-seq), 27,238 individual transcripts that were expressed in either sample. As previously reported, myogenesis is accompanied by profound transcriptional changes (Spletter et al., 2015, 2018). Consistently, we found that the expression of 10,446 transcripts was activated over time, whereas 11,376 transcripts were repressed between the two developmental points (Figure 4A; Table S2; false-discovery rate [FDR] < 0.05). To determine which of these transcripts are direct targets of Rbf and, hence, can be regulated by Rbf, we isolated chromatin from dissected IFMs of pharate adults and performed chromatin immunoprecipitation sequencing (ChIP-seq) using an Rbf antibody (Table S3). As expected, Rbf occupancy is highly enriched in the promoter and intronic regions of the gene (Figure 4B). In the promoter region, Rbf is preferentially present immediately upstream of the transcription start site (TSS; Figure 4C), which is in agreement with previous findings (Korenjak et al., 2012). We defined Rbf direct targets as transcripts in which Rbf is present nearby the TSS (region 1 kb upstream and 1 kb downstream of the TSS). Using this criterion, we found that, in mature muscles, 4,146 transcripts are direct Rbf targets (FDR < 0.05; fold enrichment ≥ 4; Table S3). Strikingly, during the normal myogenic program almost half of these mRNAs are repressed, and one-third of these mRNAs are activated (2,033 transcripts and 1,432 transcripts, respectively; Figure 4D; Table S2).

Because, in *Drosophila*, the recruitment of Rbf to chromatin is exclusively dependent on E2F (Korenjak et al., 2012), we determined the genomic occupancy of E2F in the mature muscles by ChIP-seq using the Dp antibody (Figures 4B and 4C; Table S4). Remarkably, more than 94% of transcripts identified as Rbf targets were also found to be Dp targets (Figure 4E). Accordingly, the profile of the genomic occupancy of Dp was strikingly similar to the Rbf profile (Figures 4B and 4C). This suggests that both Rbf and Dp are present near the promoters of transcripts that change their expression during normal myogenesis.

To determine the functional importance of Rbf occupancy on these promoters, we isolated RNA from the IFMs at the pharate stage after Rbf depletion with the *Mef2-GAL4* driver. We performed RNA-seq and compared the transcriptome with its matching control (Table S1). We specifically focused on the transcripts that were both direct targets of Rbf and differentially expressed upon Rbf depletion (FDR < 0.05). Among the 2,033 mRNAs that were direct targets of Rbf and were repressed during normal myogenesis, 1,146 transcripts were differentially expressed in Rbf-depleted muscles when compared with the control. Conversely, out of the 1,432 activated-Rbf direct targets, 932 transcripts were differentially expressed upon Rbf depletion (Figures 4F and 4G; Table S2). The latter was unexpected because Rbf is thought to function primarily as a repressor of gene expression, yet the depletion of Rbf prevented the activation of a large number of Rbf targets during muscle development. To analyze how the expression of these transcripts was affected in Rbf-depleted muscles, we grouped the profiles based on their change in expression by hierarchical clustering (Figures 4F and 4G). We found that many Rbf direct targets failed to be repressed (986 versus 1,146 transcripts; Figure 4F; Table S2) and failed to be activated (851 versus 932 transcripts, Figure 4G; Table S2) in Rbf-depleted muscles. The occupancy of both Rbf and Dp near the TSS of the 1,146 transcripts (Figure 4F, right) and 932 transcripts (Figure 4G, right) was visualized with ChIP-tag density plots and compared.

Next, we performed gene-ontology (GO) enrichment analysis to identify biological processes that were affected by the loss of Rbf during myogenesis (Table S5). Genes that are normally repressed by Rbf, hence, those that were increasing in Rbf-depleted muscles (Figure 4F, vertical cyan bar), were significantly enriched for the cell cycle-related categories: DNA repair, response to stress, protein-DNA complex assembly, and DNA metabolic process (Figures 5A and 5B). These results are consistent with the well-known role of Rbf as a negative regulator of cell cycle, DNA replication, and purine and pyrimidine metabolism (Dimova et al., 2003; Lewis et al., 2004; Nicolay et al., 2013). Interestingly, Rbf target genes that are activated by Rbf and were downregulated in Rbf-depleted muscles (Figure 4G, vertical magenta bar) were significantly enriched for metabolicrelated categories, including generation of energy and oxidation-reduction processes, which are known to be important for muscle development and function (Figures 5A and 5C, magenta; *P5CDh1* and *cyt-c-p* [Spletter et al., 2015, 2018]). Additionally, there were genes encoding for sarcomeric components, such as Zasp66 and Tm1, and myogenic regulators, including how and Mef2 (Figure 5C). However, we noted that the enrichment of the muscle-related GO categories was not statistically significant, suggesting that the expression of only a few myogenic genes were altered. Nevertheless, the reduction in the expression level of either a single, key myogenic factor, such as Mef2, or a crucial component of the sarcomeric structure, such as Tm1, causes severe muscle dysfunction (Bryantsev et al., 2012; Soler et al., 2012; Tansey et al., 1991).

To explore the mechanisms by which Rbf represses one group of transcripts and activates another set of transcripts, we examined the profiles of Rbf and Dp occupancy near the TSS of the Rbf targets and found no significant differences between Rbf and Dp peak profiles in these two classes of genes. Both Rbf and Dp were primarily present immediately upstream of the TSS of both the repressed and activated genes sets (Figure 5D). Next, we performed the de novo motif discovery using the parameters of the search that allowed for zero or one

occurrence per sequence and the motif length of 6–10 bp. We identified remarkably similar motifs among both repressed and activated transcripts (Figure 5E). The most-overrepresented motif was compared against the vertebrate databases of known motifs using the motif comparison tool TOMTOM, which revealed a highly statistically significant match to the E2F binding site (Figure 5E). Thus, the E2F motif is one of the prevailing elements within the promoters of genes regulated by Rbf, irrespective of whether Rbf is needed for repression or activation of gene expression. Our data are consistent with the average profile of Dp near the TSS of both transcript groups (Figure 5D).

To validate some of these targets, chromatin was extracted from pharate for ChIP-qPCR using anti-Dp and anti-Rbf antibodies. As expected, both Rbf and Dp were enriched near the TSS of some metabolic and muscle-dependent genes, including *P5CDh1, Cyt-c-p,* and *Zasp66* (Figure 5F, top and bottom). Significantly, the enrichment was largely lost in Dp-depleted animals, thus further confirming the specificity of the signal. The reduced recruitment was not due to altered levels of Rbf expression in *Mef2>Dp-RNAi* animals (Figure 5G). Note, that because Dp expression was knocked down only in muscles, there was a substantial contribution of the remaining wild-type tissue in the chromatin samples, which may explain why the loss of Rbf and Dp enrichment in the promoters was only partial after Dp depletion.

Overall, our data support the interpretation that, unlike in mammals, the role of Rbf in activating the expression of the muscle-dependent transcripts is mediated by E2F.

The Expression of Rbf Dynamically Changes throughout Muscle Development

To get insights into the function of Rbf during muscle differentiation, we systematically investigated the expression of Rbf at multiple time points during flight-muscle development with an anti-Rbf antibody (Figure 6A). Rbf was highly expressed in proliferating myoblasts at early stages of pupal development as myoblasts were migrating to fuse with forming myotubes. Strikingly, the levels of Rbf expression between the myoblasts and the developing myotubes were dramatically different. At 14 h APF, the levels of Rbf were considerably lower in myotubes compared with the surrounding pool of migrating myoblasts. The expression of Rbf remained low in myotubes until fusion was complete, and no myoblasts were detectable at 33 h APF.

To validate that the observed staining accurately reflected Rbf expression, we depleted Rbf throughout muscle development and stained dissected DLMs at 29 h APF with an anti-Rbf antibody. Rbf staining was observed in neither myoblasts nor myotubes, and yet, a strong signal was consistently detected in wild-type sample (Figure 6B). Furthermore, unlike Rbf, both E2f2 and Dp were readily detected in both proliferating myoblasts and in the nuclei of developing myotubes with no difference in their relative expression (Figures 6C and 6D). We note that the Dp antibody also revealed a nonspecific cytoplasmic staining in myotubes because it persisted in Dp-depleted muscles (Figure 6C, right). Hence, the low level of Rbf staining in myotubes is not due to the inability to detect the expression of proteins by immunofluorescence. Next, we examined Rbf expression at later stages of muscle development when the expression of sarcomeric components increases over time, as

indicated with the *Mhc>tauGFP* reporter (Figure 6E). The Rbf signal was detected in dissected DLMs at 52 h APF and remained present at 80 and 96 h APF (Figure 6E).

We concluded that actively proliferating myoblasts express high levels of Rbf, whereas the expression of Rbf is dramatically reduced as myoblasts undergo fusion to form myotubes.

Rbf Is Required to Regulate Muscle Maturation in Late Myogenesis

The results described above show that Rbf expression persists throughout myogenesis. To compare the importance of Rbf between early stages and late stages of myogenesis, the expression of Rbf was temporally and spatially restricted using the TARGET system (McGuire et al., 2004). Rbf was depleted in muscles using the *Mef2-GAL4* driver at different time points with the temperature-sensitive GAL4 repressor ($GAL80^{TS}$; Figure 7A, left). *Rbf-RNAi* was induced at 31°C by inactivating GAL80*TS*, and thus, allowing GAL4 expression. Conversely, at 18°C, GAL80*TS* is functional, and therefore, *Rbf-RNAi* is no longer active. The animals with *Mef2>Rbf-RNAi, Dicer2,* and $GAL80^{TS}$ raised at 31°C throughout development showed about 50% lethality during pupa development (Figure 7A, right). When the system was switched OFF (*Rbf-RNAi* was no longer induced at 18°C) at either mid or early pupa development, animals displayed the phenotype, suggesting that Rbf is required during pupal development. However, when the system was switched OFF earlier, immediately preceding pupa formation (larvae were moved to low temperature at late third-instar development), no lethality was detected, thus implying that the loss of Rbf in proliferating myoblasts during larval stages is not detrimental to development. Hence, Rbf function appears to be more relevant at later stages of myogenesis than at earlier stages.

To confirm the importance of Rbf during late myogenesis, we depleted Rbf using a late muscle driver, *Act88F-GAL4*. This driver is expressed in the postfusion IFMs, at the onset of myofibril formation (Bryantsev etal., 2012). The overall structure of myofibrils was examined in sagittal sections of *Act88F>Rbf-RNAi;Dicer2* adults and compared to controls. Interestingly, myofibrils failed to display a repetitive organization in Rbf-depleted myofibers (Figure 7B). Most thoraces showed disorganized and wavy myofibrils, and in some cases, a frayed phenotype was detected, in which sarcomeres were barely visible (Figure 7B, bottom). To determine the significance of these defects, we assessed overall muscle function in Rbf-depleted myofibers with a flight test assay. In this assay, animals that fly land on the top of the cylinder walls, whereas flightless flies land at the bottom. Notably, Rbf-depleted animals were flightless compared with controls (Figure 7C). Thus, Rbf is required during the stage of muscle maturation to promote proper myofibril and sarcomere assembly, which is needed for proper muscle function.

Rbf Interacts with Other Transcription Factors during Myogenesis

In mammals, pRB interacts with tissue-specific transcription factors other than E2F to promote differentiation (Novitch et al., 1999; Schneider et al., 1994; Thomas et al., 2001). In addition to the E2F binding sites, several additional DNA motifs were identified in the sequences around Rbf peaks. The motifs were matched against *Drosophila* and vertebrate databases of known motifs using the motif comparison tool TOMTOM. Among the transcripts repressed by Rbf (Figure 7D, left), we identified the binding site for the DNA

replication-related element factor (Dref), which functions synergistically with an E2F-binding site and is commonly found in the promoters of proliferation-related genes (Hirose et al., 1993). We also found a motif match for the insulator protein BEAF-32. BEAF-32 cooperates with an E2f2/Rbf repressor complex dREAM to block the activity of the adjacent enhancers (Korenjak et al., 2014).

When the parameters were adjusted to allow for any number of repeats per sequence, and the motif length was between 6 and 14 bp, the binding sites of ESR1/2 and CUX1 were identified in the promoters of Rbf-activated transcripts (Figure 7D, right). The *Drosophila* orthologs are estrogen-related receptor (ERR) and hormone receptor 83 (Hr83) for the former motif, and cut (ct) for the latter. To further investigate what other transcription factor binding sites are differentially enriched between activated and repressed transcripts, we used the bioinformatics tool STORM to determine the occurrence of the regulatory motif near the Rbf peak summit. The occurrence of the motifs ultraspiracle (usp), signal-transducer and activator of transcription protein at 92E (Stat92E), and delta (Dl) was about two times greater in the Rbf-activated transcripts compared with the Rbf-repressed transcripts (Figure 7E).

The importance of these sequence motifs in the promoters of Rbf targets was functionally evaluated with genetic-interaction tests. We asked whether knocking down any of the transcription factors that we identified above enhanced the lethal phenotype of *Mef2>Rbf-RNAi* animals. To increase the range of this Rbf-dependent phenotype, we removed *UAS-Dicer2* to allow *Mef2>Rbf-RNAi* animals to survive through adulthood (Figure 7F). The knockdown of *usp, ct*, and *Stat92E* resulted in the lethality of otherwise viable *Mef2>Rbf-RNAi* animals (Figure 7F). Significantly, the lethal phenotype was enhanced compared with the effects of the knockdown of each transcription factor alone without Rbf (Figure 7F). In contrast, other transcription factors, including Dl and ERR, did not enhance Rbf-dependent phenotype in this assay (Figure S2). To control for RNAi specificity, these tests were repeated with several independent RNAi lines.

These results suggest that *usp, ct,* and *Stat92E* are important in adult skeletal muscles. To further explore this idea, we depleted these transcription factors with *Act88F-GAL4* and performed a flight test as a readout of flight-muscle function. Notably, the loss of usp led to lethality, and the loss of ct significantly impaired flight ability (Figure 7G), whereas Stat92E and Dl affected the adults to a lesser extent, and ERR did not affect them. Because the animals *Act88F>Rbf-RNAi* are already flightless (Figure 7C), it precluded us from testing whether Rbf genetically interacts with those transcription factors in this assay.

We concluded that *usp, ct,* and *Stat92E* are important for Rbf function during late myogenesis. Given that the binding sites for these factors occur more frequently at the promoters of transcripts activated by Rbf, we suggest that the interaction between Rbf and these DNA-binding factors may have a role in Rbf-dependent gene activation.

DISCUSSION

In this study, we addressed a long-standing question about the role of pRB in terminal differentiation during animal muscle development. We show that the inactivation of Rbf, the *Drosophila* pRB homolog, results in severe abnormalities in skeletal muscle formation without concomitant ectopic cell cycles. Notably, these structural defects are accompanied by the failure to activate expression of late-myogenic genes during muscle maturation. Our data suggest that Rbf is required for the activation of the myogenic transcriptional program and genetically interacts with other transcription factors, such as usp, ct, and Stat92E. Thus, in addition to the canonical function of Rbf as a transcriptional repressor, we identified the specific developmental context in which Rbf operates as an activator of gene expression (Figure 7H).

There is ample evidence that the ablation of RB affects muscle development. For example, $Rb1^{-/-}$ mouse embryos that are partially rescued to birth by low levels of *Rb1* expression or by a wild-type placenta exhibit reduced skeletal muscle mass and disorganized myofibril structure (de Bruin et al., 2003; Zacksenhaus et al., 1996). However, this defect is accompanied by high levels of both apoptosis and ectopic cell cycles, which complicate the interpretation of the phenotype. In flies, the inactivation of Rbf similarly affects cell proliferation, but these defects are restricted to early stages of myogenesis when myoblasts are actively dividing. Rbf-depleted myoblasts exited the cell cycle on time, and no ectopic cell divisions were detected thereafter. Thus, the number of nuclei per muscle was not significantly impaired. Therefore, the loss of Rbf during myoblast proliferation has no significant effect in myogenesis. This observation is consistent with previous reports showing that cell cycle exit upon terminal differentiation remains largely unperturbed in *Rbf*-mutant cells or in cells that overexpress E2f1 (Buttitta et al., 2007; Firth and Baker, 2005). Thus, *Drosophila* provides a powerful system to examine the *bona fide* role of Rbf in myogenesis without unwanted effects associated with ectopic cell proliferation.

The analysis of the Rbf-depleted muscles led to two important findings. First, the depletion of Rbf results in the reduction of the muscle size along with defects in the formation of the sarcomeric structures. Although this phenotype may arise from defective tension during muscle attachment at the onset of myofibrillogenesis, the results of Rbf depletion with the late muscle driver argue that Rbf is directly involved in late-muscle maturation. Second, we show that Rbf activates the myogenic transcriptional program. This conclusion is supported by integration of RNA-seq and ChIP-seq, which identified a large group of direct Rbf targets that failed to be induced upon Rbf depletion. Among them are genes encoding components of the sarcomeric complexes and myogenic regulators, which may help to explain the observed defects in muscle maturation. Rbf was also required for the proper activation of the metabolic genes. In concordance with our results, pRB has been linked to the regulation of the metabolic function in other systems (Dyson, 2016). pRB is required for the expression of genes involved in mitochondrial oxidative metabolism, glucose, and fatty acid metabolism in differentiated C2C12 myotubes (Petrov et al., 2016) and was shown to regulate oxidative phosphorylation genes in muscle and brown adipose tissue in mice (Blanchet et al., 2011). In *Drosophila*, the loss of Rbf was shown to have a profound effect on glutamine metabolism (Nicolay et al., 2013). Altogether, our data provide a simple explanation that the reduced

size of Rbf-depleted muscles is likely due to the failure to properly upregulate the myogenic transcriptional program.

In *Drosophila*, Rbf is thought to operate primarily as a transcriptional repressor (Dimova et al., 2003; Georlette et al., 2007; Korenjak et al., 2012). These genome-wide studies profiled either the entire animals or cultured cells. Thus, a particular differentiation program executed in a few cells could be missed. Here, we used dissected adult skeletal muscles for both RNA-seq and ChIP-seq. This allowed us to identify an Rbf-specific transcriptional program that operates *in vivo* during muscle differentiation.

One of the outstanding questions is how Rbf activates transcription during myogenesis. Mammalian pRB was implicated in potentiating the activity of tissue-specific factors, such as myogenin and MEF2C in cultured myotubes cells (Novitch et al., 1999; Schneider et al., 1994) and CBFA-1 in Saos-2 cells (Thomas et al., 2001), and to interact with the histone demethylase KDM5A (Benevolenskaya et al., 2005). These interactions were shown to be important for the expression of late-differentiation markers. The analysis of Rbf-bound regions from our ChIP-seq experiment revealed an E2F binding site as the prevailing motif for both the activated and the repressed transcripts. Consistently, there was a remarkable overlap between the occupancy profiles of Dp and Rbf in muscles. In addition, the occupancy of Rbf at several myogenic genes was largely abolished in Dp-depleted muscle (this work and Zappia and Frolov [2016]). Thus, in *Drosophila*, the activation of the myogenic genes by Rbf is likely to be E2F dependent. This is consistent with previous work, in which genomic targeting of Rbf occurred entirely via E2F/Dp (Korenjak et al., 2012). In agreement with this idea, the inactivation of E2F by depleting Dp phenocopies the inactivation of Rbf in muscles (Zappia and Frolov, 2016). However, we cannot completely exclude the possibility that the effects of Dp and Rbf depletion may be different on some promoters. One surprising implication of these results is that E2f1 alone, in the absence of Rbf, is unable to activate the myogenic genes. We note that E2f1 can still activate transcriptions at this time point because the cell cycle E2F targets are upregulated in Rbf-depleted muscles. Therefore, the role of Rbf as a positive regulator of gene expression appears to be limited to genes involved in differentiation. Intriguingly, mammalian pRB functions by reversing the repression of the histone demethylase KDM5A at the promoters of the nuclear encoded-mitochondrial genes during differentiation (Varaljai et al., 2015). Because we found that Rbf is similarly needed for the activation of the metabolic genes including OXPHOS genes during muscle differentiation, it may be interesting to explore whether this mechanism is conserved.

Remarkably, there is an abrupt change in the levels of Rbf protein between proliferating myoblasts and growing myotubes. This raises the possibility that Rbf is degraded upon myoblasts fusion and, perhaps, a newly appearing pool of Rbf that activates transcription during muscle growth and maturation. Indeed, a proteasome-mediated degradation of Rbf has been previously suggested to be linked to developmental signals (Acharya et al., 2010). Notably, another myogenic regulator, the RNA-binding protein Arrest, shuttles into the nuclei of DLMs at the onset of muscle maturation (Spletter et al., 2015). Thus, changes in the levels or localization of myogenic regulators could be a common feature.

Interestingly, about three-quarters of the transcripts that are directly regulated by Rbf in IFMs are also Rbf targets in larvae (Korenjak et al., 2012). Concordantly, we have previously detected Rbf near the TSS of several muscle-specific genes, including *Tm1, how, fln, Mef2, Lmpt,* and *sals* in larva (Zappia and Frolov, 2016). Thus, Rbf occupancy at myogenic genes does not appear to correlate with the timing of their activation, suggesting that the presence of Rbf alone is not sufficient to activate their transcription. One possibility is that Rbf may assist other transcription factors in the regulation of the myogenic transcriptional program. This idea is supported by the identification of the binding sites of five transcriptional factors near the Rbf peak summits, which are specific for Rbf-activated transcripts. Intriguingly, three of them, usp, ct, and Dl, were identified in the large-scale screen for genes required for muscle morphogenesis and function (Schnorrer et al., 2010), albeit their precise role has not been determined. Other studies reported the role of Stat92E in somatic muscle development in embryo (Liu et al., 2009) and the involvement of ct in the diversification of myoblast that give rise to different types of flight muscles (Sudarsan et al., 2001). Accordingly, we show that the knockdown of usp, ct, Stat92E, and Dl with the late muscle-driver *Act88F-GAL4* impairs the ability of animals to fly, thus indicating their requirement in flight-muscle function. Notably, only three of these genes, usp, ct, and Stat92E, enhance the Rbf-dependent muscle phenotype, thus confirming the specificity of the genetic interactions between these factors and Rbf. These results raise the possibility that Rbf may interact with these factors to regulate the muscle-specific transcriptional program.

Unlike mammals, in which pRB directly interacts with such factors to potentiate their activity, in *Drosophila*, the recruitment of Rbf to myogenic genes is likely mediated by E2F. Nevertheless, the overall arrangement appears to be highly similar as both pRB and Rbf function to help the activation of specific transcriptional programs to promote differentiation. Given such remarkable conservation, *Drosophila* may prove to be a powerful system to investigate the role of the retinoblastoma protein in the context of differentiation regulation.

STAR★METHODS

CONTACT FOR REAGENT AND RESOURCE SHARING

Further information and requests for resources and reagents should be directed to and will be fulfilled by the Lead Contact, Maxim V. Frolov (mfrolov@uic.edu).

EXPERIMENTAL MODEL AND SUBJECT DETAILS

Fly stocks—The line *Act88F-GAL4* (Bryantsev et al., 2012) and *P{twi- bgal}* were provided by Richard. M. Cripps. The stock vgAME-lacZ was used to mark the developing indirect flight muscles. The GAL4 drivers *P{GawB}how24B* and *P{GAL4-Mef2.R}*3, and the GFP reporter for Mhc expression *P{Mhc-tauGFP}*2 were obtained from Bloomington *Drosophila* Stock Center (Bloomington, IN, USA). The lines *UAS-Rbf-RNAi* and *UAS-Dp-RNAi* were obtained from the library RNAi-GD (ID 10696 and 2722, respectively) at the Vienna *Drosophila* Resource Center (Vienna, Austria). The stocks *P{VALIUM20-mCherry}attP*2, and *P{VALIUM20-EGFP.shRNA.3}attP40* from TRiP collection was used as control, and *P{UAS-Dcr-2.D}* was used to help processing long, partially double-stranded

endogenous transcripts (hairpin RNAs) into endo-siRNAs. In all experiments the transgene *UAS-Dicer-2* was added to enhance the Rbf-dependent phenotype, except Figure 7F. These stocks were obtained from Bloomington *Drosophila* Stock Center. All fly crosses were made at 25 C in vials containing standard cornmeal- agar medium.

Rbf was depleted in muscles using *Mef2-GAL4* and regulated over time with the TARGET system (McGuire et al., 2004). *P{tubP-GAL80[ts]}20* was inactivated in water bath at 31 °C whereas it was fully active in incubator set at 18°C. l Females laid eggs for a period of 24 h at 18°C. Animals were kept at 18°C during embryogenesis. Then, vials were placed at 31 °C during larval development to switch ON the TARGET system to inactivate *GAL80[ts]* and release the inhibition on GAL4 activity. The system was switch OFF (back at 18°C) at mid pupa development (approx. 36 h APF), early pupa development (around 0 h APF), and late third instar larva. Additionally, the system was kept either ON (31 °C) or OFF (18°C) during development to control GAL80 activity.

Two RNAi lines were used for usp (1: UAS-usp-RNAi^{GD1554} and 2: UAS-usp-RNAi^{JF02546}), one for UAS-ct-RNAi^{GD1237}, and two for Stat92E (1: UAS-Stat92E-RNAi^{HMS00035} and 2: UAS-Stat92E-RNAi^{JF01265}), three for ERR (1: UAS-ERR-RNAi^{HMJ23520}, 2: UAS-ERR-RNAi^{JF02431} and 3: UAS-ERR-RNAi^{HMC03087}), and two for Dl (1: UAS-Dl-RNAi^{GD1238} and 2: UAS-Dl-RNAi^{JF02825}). All these RNAi lines were obtained from Bloomington *Drosophila* Stock Center expect UAS-usp-RNAi^{GD1554}, UAS-ct-RNAi^{GD1237} and UAS-Dl-RNAi^{GD1238}, obtained at the Vienna ^{Drosophila} Resource Center (Vienna, Austria).

Cell culture, dsRNA and myotube differentiation—*Drosophila* ML-Dmd8 cells (RRID:CVCL_Z754) were maintained at 25°C in Schneider's *Drosophila* Medium (GIBCO, 2018-03) supplemented with 10% v/v fetal bovine serum (FBS, Hyclone) and 10 μg/ml insulin (Sigma, I0516).

dsRNA knockdown was done by soaking cells with 50 μg of dsRNA targeting GFP and Rbf in serum-free media for 4 h in six-well plates, after which complete media was added. Two days after dsRNA treatment, cells were re-plated into 24-well plates and resoaked with dsRNA. Then growth medium was switched to differentiation medium to induce differentiation. Sequences of primers used to synthesize dsRNA are listed in Table S7.

Differentiation into myotubes was induced by seeding cells at 5,000 cells/mm^2 with the growth medium, which contains 10% FBS supplemented with 10 μg/ml insulin in Schneider's. Media was changed 2 hours after seeding when cells reached 100% confluence. Differentiation medium composition was Schneider medium with 2% v/v horse serum (GIBCO, 16050-122), 10 μg/ml insulin, and ecdyson 1 μM (20-Hydroxyecdysone, Sigma). Media was changed every 24 h. In all experiments, Day 0 is 10% FBS, 10 μg/ml insulin, and 1 μM ethanol in Schneider medium

METHOD DETAILS

Fly viability assay—Crosses were set at 25°C and the development of animals was kept at 25°C, expect in the experiment in which GAL80^{TS} was used. The total number of pupa, as

well as pharate pupa, and adult flies able to eclose out of the pupal case were scored over time. The pupal developmental stages were assessed by following markers of metamorphosis. The percentage of animals scored at each developmental stage was plotted (Adults, Pharate and Early pupa). At least 52 flies per genotype were scored in two independent experiments.

Flight test—Adult females were collected on eclosion and recovered at 25 C for 4–6 days. A 2,000 mL cylinder was coated with mineral oil. Flies were flipped to the top of the column. Flies that are able to fly land on the top section of the column, while flightless flies fall to the bottom of the cylinder. The landing spot along the height of the cylinder was scored for each fly, and the frequency of landing spots per height of the cylinder was plotted. At least 80 flies per genotype were tested in each experiment. Each experiment was carried out two times.

In the case of the genetic interaction experiments, male were collected and the cylinder was divided into three sections (top middle and bottom). The percentage of flies landing to each section of the cylinder was scored. At least 180 flies per genotype were tested in each experiment. Each experiment was carried out two times.

Immunofluorescence and confocal microscopy—ML-Dmd8 cells seeded in 12mm poly-L-lysine coated round coverslip (Fisher Scientific, 08-774-384) in a 24-well plate were harvested at day 0, 3 and 6 post-differentiation. Cells were washed with PBS 1x, fixed in 4% formaldehyde for 15 min, washed with PBS, and blocked in 3% bovine serum albumin (BSA) with 0.5% Triton X-100 for 30 min. Cells were incubated with antibodies for 2 h in a humid chamber in 1% BSA. After washing three times for 5 min each in PBS, cells were incubated with appropriate Cy3- or Cy5-conjugated anti-rabbit secondary antibodies (Jackson Immunoresearch Laboratories, used at 1:500) for 30 min in 1% BSA. After washing three times with PBS, coverslips were mounted with FluorSave Reagent (Calbiochem, 345789) on glass slides.

Tissues were dissected and immediately fixed in 4% formaldehyde in PBS for 30 min, permeabilized in 0.3% Triton X-100 in PBS twice for 10 min each and blocked in 2% bovine serum albumin (BSA) with 0.3% Triton X-100 in PBS for 60 min. The DLMs of pupa staged at 15, 20, 21, 24, 29 and 33 h APF were dissected as in (Weitkunat and Schnorrer, 2014), fixed for 20 min, and washed in PBS with 0.1% Triton X-100. Thoraces of 2- to 5-day-old adult or pharate pupa staged at 43, 52, 72, 80 and 96 h APF were fixed for 1 h in relaxing buffer. Thoraces were bisected in the sagittal plane, and were then fixed for an additional 15 min as described in (Schnorrer et al., 2010). In the case of transverse plane sectioning, flies were snap-frozen in liquid nitrogen and cut twice with a razor. The transverse sections were fixed for 1 h. A minimum of five to eight animals per genotype was dissected per experiment, except for the experiment that required quantitative analysis, in which case the staining was carried out two or three times.

Samples were incubated with antibodies overnight at 4°C in 2% BSA and 0.1% Triton X-100 in PBS. After washing four times for 10 min each in 0.1% Triton X-100 (in PBS), samples were incubated with appropriate Cy3- or Cy5-conjugated anti-mouse and anti-rabbit

secondary antibodies (Jackson Immunoresearch Laboratories, used at 1:300) for 90 min in 10% normal goat serum and 0.1% Triton X-100 in PBS. After washing with 0.1% Triton X-100 (in PBS), tissues were stored in glycerol with antifade, and then mounted on glass slides. All steps were performed at room temperature, unless otherwise stated.

The primary antibodies were mouse anti-β-Gal (40-1a, 1:200, Developmental Studies Hybridoma Bank (DSHB)), mouse anti-β-PS-integrin (*CF*.6G11,1:50, DSHB), mouse 22c10 (1:30, DSHB), rabbit anti-Mef2 (1:1,000) (Lilly et al., 1995), mouse RBF (DX2, 1:20, (Du et al., 1996), rabbit polyclonal anti-Dp (#212, 1:300)(Dimova et al., 2003), rabbit anti-E2f2 antibodies (#79), rabbit anti-Cleaved *Drosophila* Dcp-1 (Asp216, 1:500, Cell Signaling), rat anti-Kettin (MAC155,1:1000, Babraham Institute) and rabbit anti-pH3 (Millipore, 1:200), Rhodamine–Phalloidin or fluorescein isothiocyanate–Phalloidin were used to counterstain and stain thin filaments, and 4,6-diamidino-2-phenylindole (DAPI) for nucleus staining. *Mef2>Dp-RNAi* was used as negative control because of the non-specific background signal detected in the cytoplasm of myotubes.

Fluorescent images were acquired with the laser-scanning confocal microscope (Zeiss LSM Observer.Z1) using ×20/0.8, ×40/1.2 and ×100/1.45 objectives. Images were processed using Photoshop (Adobe Systems). All images are confocal single-plane images, unless otherwise stated. Only representative image is shown per experiment.

Western blot—Six or eight pharate pupae (96 h APF) were collected per sample by removing the pupa case. Flight muscles were dissected from 15-20 thoraces of pharate pupa (96 h APF) in relaxing buffer, snap-freezed in dry ice, and homogenized in 40 μL or 100 μL of lysis buffer (50mMHEPES[pH8.0], 100mMKCl, 2mM EDTA, 10%glycerol, 10 mM NaF, 1 mM dithiothreitol [DTT], 1 mM phenylmethylsulfonyl fluoride [PMSF], 0.1% NP-40, protease inhibitor cocktail (Sigma)).

ML-Dmd8 cells were plated in a 12-well plate and soaked with 20 μg dsRNA as previously described here. Cells were harvested 4 days post-treatment, span down for 2 min at 4000 rpm in a refrigerated centrifuge. Samples were homogenized in 80 μL of lysis buffer. Bradford method was used to estimate protein content in each sample. Between 15 and 20 μg of sample was loaded by well using laemmli loading buffer. Proteins were resolved by electrophoresis on a sodium dodecyl sulfate 8% and 10% polyacrylamide gel electrophoresis gel. Membranes were probed with mouse anti-E7 (β-tubulin, 1:7000, DSHB), or mouse anti-RBF (DX3, 1:5) (Du et al., 1996). Goat anti-mouse secondary antibody conjugated with horseradich peroxidase was used (1:5000). The blots were developed with Pierce ECL kit (Thermofisher).

RNA-seq and RT–qPCR

Sample preparation: Wandering third instar larvae were harvested, wing discs were dissected, and notum was cut and collected. Flight muscles were dissected from female pharate animals at 96 h APF. At least three to five pharates, and between 11 and 15 third instar larvae were dissected per sample. ML-Dmd8 cells were seeded in a 24-well plate, and harvested after 0, 3, 6 and 9 days of differentiation using TRIzol™ Reagent (Invitrogen).

Two or three independent biological samples were collected for each genotype and developmental stage, or treatment condition. Total RNA was isolated with TRIzol.

RNA-seq libraries and sequencing: Samples were submitted to the Genomics Facility at the University of Chicago, Chicago, IL, for DNase treatment, generation of total RNA libraries (Ribo-Zero depletion) using Illumina TruSEQ Stranded kits, and sequencing using Illumina HiSEQ4000. Illumina bcl2fastq2-v2.17.1.14 software was used for basecalling.

Read Quality Assessment and Filtering: Basic assessment of Illumina output reads (FastQ) quality including GC bias were checked by FastQC program (https://www.bioinformatics.babraham.ac.uk/projects/fastqc/). Poor quality reads were eliminated before mapping based on default quality flag by Illumina pipeline in FastQ file.

Mapping of reads: Mapping of reads was done with TopHat (tophat version 2.1.1 with Bowtie version 2.3.2) (Trapnell et al., 2009). Identified 50bp short reads were uniquely aligned allowing at best two mismatches to the *Drosophila melanogaster* reference genome from Ensembl database (BDGP5.77) (Hubbard et al., 2007). Sequence matched exactly more than one place with equally quality were discarded to avoid bias. The reads that were not mapped to the genome were utilized to map against the transcriptome (junctions mapping). EnsEMBL version 77 (Hubbard et al., 2007) gene model was used for this process.

Read count, normalization and differential expression analysis: After mapping, we used SubRead package featureCount (version 2.21) (Liaoet al., 2013) to calculate absolute read abundance (read count, rc) for each transcript/gene associated to EnsEMBL (v77) genes of *D. melanogaster*. For differential expression (DE) analysis by popular bioconductor package DESeq2 (version 1.14.1) with R version 3.3.2 (2016-10-31) (Anders and Huber, 2010) that uses a model based on the negative binomial distribution. To avoid false positive, we considered only those transcripts where at least 10 reads are annotated in at least one of the samples used in this study. Heatmap were generated using Genesis platform ((Sturn et al., 2002). A hierarchical unsupervised clustering was applied using Pearson correlation distance. List of genes and transcripts were compared using Venn diagram from Venny 2.1.

RT-qPCR: Reverse transcription to measure standard mRNAs was performed using the SensiFAST cDNA Synthesis Kit (Bioline) according to the manufacturer's specifications. qPCR was performed with the SensiFast SYBR No-ROX Mix (Bioline) on a LightCycler 480 (Roche). The reference genes RpL32, RpL30 were validated as stable control genes. Normalization was calculated using the geometric mean of these reference genes. Primer sequences are listed in Table S7. Each sample was measured twice. In all experiments normalized data is relative to control (Day 0, *GFP*-dsRNA, *Mef2>mCherry-RNAi*)

ChIP-seq

Sample preparation: Flight muscle tissues were dissected out of at least 35 pupae staged at pharate (96 h APF) and homogenized. Control genotype was used *Mef2>mCherry-RNAi.* Chromatin was extracted using homogenizer with 60 mM KCl, 15 mM NaCl, 4 mM

MgCl2,15 mM HEPES (pH 7.6), 0.5% Triton X-100, 0.5 mM dithiothreitol (DTT), 10 mM sodium butyrate and protease inhibitor cocktail (Complete, Roche). Samples were crosslinked for 15 min at room temperature in 1.8% formaldehyde, and 225 mM Glycine was added. Then, cells were lysed with 15 mM HEPES at pH 7.6, 140 mM NaCl, 1 mM EDTA, 0.5 mM EGTA, 0.1% sodium deoxycholate, 1% Triton X-100, 0.5 mM DTT, 0.1% SDS, 0.5% lauroylsarcosine and 10 mM sodium butyrate with protease inhibitor cocktail (Complete, Roche), and were sheared using a Branson 450 Sonifier. Chromatin was immunoprecipitated with mouse anti-Rbf (DX3/DX5, ratio 1:1) (Du et al., 1996) and anti-DP (#212, (Dimova et al., 2003)). Complexes were pulled down with Protein G Dynabeads (Invitrogen), washed with lysis buffer four times, washed twice with TE (pH 8), eluted and decrosslinked overnight at 65°C; RNA was degraded with RNase A (Sigma) for 1 h at 37°C and protein was digested with proteinase K for 2 h at 50°C. DNA was purified by phenol–chloroform extraction, followed by overnight ethanol precipitation. Two independent biological samples were used.

ChIP-seq libraries and sequencing: Samples were submitted to the Genomics Facility at the University of Chicago, Chicago, IL. ChIP-seq libraries were generated using an Illumina ChIP-SEQ kit, and sequenced using Illumina HiSEQ2500 (v4 chemistry). Illumina bcl2fastq-1.8.3 software was used for basecalling.

ChIP-seq data analysis: Illumina pipeline analyzed short reads were uniquely aligned allowing at best two mismatches to the reference *Drosophila melanogaster* genome version BDGP 5.77, using the program BOWTIE (version 2.3.2) (Langmead et al., 2009). Peak caller algorithm MACS (version 1.4.2) (Zhang et al., 2008) was used to determine enriched peak region with parameters:–nomodel,–tsize = 50,–shift size = 160. Shift size was determined using Pyicos (Althammer et al., 2011) strand correlation method.

Enriched peaks were annotated to all EnsEMBL (Hubbard et al., 2007) transcripts (for *Drosophila* EnsEMBL Biomart version 77) using bedTools (Quinlan and Hall, 2010) within a 5Kb window.

Distribution of enriched reads along the genome and transcription start site (TSS) of RefSeq transcripts were determined using CEAS (Shin et al., 2009). Read density graph or average profile of reads around TSS or any particular genomic location is based on “sitepro” script of the CEAS tool.

Rbf transcript targets were defined as direct targets if Rbf occupancy is enriched within −1 Kb to + 1 Kb from TSS (Transcription start site). Dp direct targets were defined the same way.

Tag density heatmaps around the transcript start site (TSS) were prepared using program HOMER (version 4.9) (Heinz et al., 2010) with parameter (-size −5000,5000 -hist 25 -ghist) and image visualize using gitools (Perez-Llamas and Lopez-Bigas, 2011).

ChIP-qPCR—Animals staged at pharate (96 h APF) were dissected out of their pupa case and homogenized. Genotype used were *Mef2>mCherry-RNAi* and *Mef2>Dp-RNAi*.

Chromatin was extracted and immunoprecipitated as mentioned earlier. In addition to mouse anti-Rbf (DX3/DX5, ratio 1:1) (Du et al., 1996) and anti-DP (#212, (Dimova et al., 2003), both mouse anti-Myc (9e10) and rabbit IgG (Sigma) were used as non-specific antibodies. The input genomic DNA (before precipitation), as well as immunoprecipitated DNA, was quantified using qPCR as described earlier. Primer sequences are in Table S7. A negative sequence site that does not contain any predicted E2F-binding sites was used as control. The protein enrichment was calculated as the percentage of immunoprecipitated DNA relative to input DNA (prior DNA precipitation) for each antibody. Data presented are relative to the negative binding site for each ChIP. Each sample was measured twice.

Next-generation sequencing data visualization—Data from ChIP-seq and RNA-seq were integrated and visualized using Integrative Genomics Viewer (IGV_2.3.79, (Robinson et al., 2011). The reads assembled were uploaded as BedGraph for RNA-seq and as bigWig format for ChIP-seq. DmBDGP5.77 used as genome annotation.

De novo motif discovery—To determine an over-represented short sequence motif in enriched peak, we used total 100 nucleotide sequence (from peak summit, 50bp down and 50bp up). We used MEME (Bailey and Elkan, 1994) program for finding enriched motif. For E2F motifs zero or one occurrence per sequence was set and motif length was 6-10 bp (Figure 5E). To discover new motifs we used zero or one occurrence per sequence and motif length 6-10 bp in transcripts repressed by Rbf; any number of occurrences per sequence and motif length 6-10 bp and 6-14 bp for transcripts activated by Rbf (Figure 7D). Tomtom was used to compare the motifs against a database of known motifs from both Eurakyote DNA (Vertebrates *in vivo* and *in silico*) and FLY DNA. E values lower than 0.01 were considered as a match.

STORM—Possible occurrence of transcription factor motif in 350bp or 550 bp of peak summit centered location (175 bp up and 175 bp down, and 275 bp up and 275 bp down) were predicted with STORM algorithm (Schones et al., 2007) with a p value cutoff determined based on the size of the input sequence as (1/100xsequence-size), and using position frequency matrices (PFM) from Transfac database (insect metrix) (professional version release 2009.4).The percentage of motif matching with each transcription factor was calculated for each set of sequence (activated and repressed by Rbf). The ratio of % transcription factor in activated over repressed was determined.

Functional Enrichment Analysis—The list of transcripts repressed and activated by Rbf, as defined in Figure 5, were annotated to genes. Functional annotation is based on Gene Ontology (GO) (Ashburner et al., 2000;http://www.geneontology.org) as extracted from EnsEMBL (Hubbard et al., 2007). Accordingly, all genes are classified into the ontology: genes involved in Biological Process (BP). We have taken only the GO/pathway categories that have at least 10 genes annotated. We used Gitools for enrichment analysis (Perez-Llamas and Lopez-Bigas, 2011) (http://www.gitools.org). Resulting p values were adjusted for multiple testing using the Benjamin and Hochberg's method of False Discovery Rate (FDR)(Benjamini and Hochberg, 1995). Enrichment map were visualized using Cytoscape v3.3.0 platform (Shannon et al., 2003). The parameters were set as $p < 0.005$, FDR < 0.05,

Similarity threshold between nodes:0.3. Flybase was used for online resources on Database of *Drosophila* Genes & Genomes.

QUANTIFICATION AND STATISTICAL ANALYSIS

Scripts were used in ImageJ for automatic and unbiased quantification, and are available upon request—Graphs were generated with the GraphPad Prism version 7.0 (Graphpad Software). The group means were analyzed for overall statistical significance using two-way analysis of variance and non-parametric analysis (Mann–Whitney).

Quantification of mitotic myoblasts and total number—The total number of mitotic myoblasts was determined using phosphorylated histone H3 antibody. The myoblast-positive area and developing DLMs area were marked with *twi-lacZ* reporter in the wing disc in late third instar larvae (120 h after egg-laying), and in pupa thoraces staged at 15, 20, 24, 29 and 33 h APF. Developing DLMs area was also labeled using 22C10 marker in pupa thoraces staged at 21 h APF, and Phalloidin in 29 and 33 h APF. Images were taken with confocal microscopy in a z stack to cover all nuclei in the tissue, and then were projected into a single plane. The area covered by the adult myoblasts and developing DLMs was quantified using the ImageJ software (1.48v, NIH, USA). The plugin Image-based Tool for Counting Nuclei was used to determine the number of pH3-positive nuclei in the myoblast-positive area and developing DLM. To count the total number of myoblasts in the wing discs a mask was created with *twi-lacZ* marker around the area of the adult muscle precursors to limit DAPI count to myoblasts. Minimum of 5 animals per genotype and developmental stage were scored. Two independent experiments, only one shown, except for Rbf-depleted DLMs staged at 29 and 33 h APF. More details regarding the statistical analysis and sample size for each experiment can be found in legend of Figure 2.

Quantification of number of nuclei in muscles—The number of nuclei, the average size of nuclei and the cross-section area of DLM in transverse sections of pharate was quantified using the Analyze particle function of ImageJ Student's. Briefly, the full area of DLM number 4 was selected as the region of interest using β-PS integrin. Then, an automatic threshold was applied to DAPI channel. Watershed segmentation was then performed to separate overlapping spots, and the total number of particles was counted along with the average size of particles and the area selected. Nine animals per genotype were scored. More details regarding the statistical analysis and sample size for each experiment can be found in legend of Figure 3.

Quantification of fiber length—ImageJ was also used to quantify muscle fiber length of DLMs in pupa thoraces staged at 29 h APF. Minimum of 5 animals per condition were scored. Two independent experiments were done, only one representative experiment shown. More details regarding the statistical analysis and sample size for each experiment can be found in legend of Figure 3.

Quantification of myofibril morphology—Images of the DLM sagittal section were blindly scored as either frayed, trapezoid or wild-type regarding myofibril morphology as in (Schnorrer et al., 2010). At least 6 hemithoraces were scored per genotype/gender/

experiment. Two independent experiments were conducted. More details regarding the statistical analysis and sample size for each experiment can be found in legend of Figure 7.

Quantification of Dmd8 cells—The number of Mef2-positive nuclei and pH3-postive nuclei in differentiating ML-Dmd8 cells were counted using the Analyze particle function of ImageJ Student's. Briefly, automatic thresholds were applied to red channels (either Mef2 or pH3), and the green channel (Phalloidin) was inverted and subtracted from the red channel to select only Mef2 and pH3 spots within cells stained with Phalloidin. Watershed segmentation was then performed to separate overlapping spots, and total number of particles was counted. Same procedure was applied to blue channel (DAPI) to count total number of nuclei to normalize data. Total number of nuclei per myotube, defined as the fusion index to characterize the efficacy of differentiation, was also quantified using ImageJ. A mask was created using Phalloidin around each myotube to limit particle count to each myotube. At least ten images per treatment/time point/experiment were processed. Three independent experiments were done. More details regarding the statistical analysis and sample size for each experiment can be found in legend of Figure 1.

DATA AND SOFTWARE AVAILABILITY

Both ChIP-seq and RNA-seq data from this publication have been deposited to the GEO database (https://www.ncbi.nlm.nih.gov/geo/) and assigned the identifier Series GSE102105 (https://www.ncbi.nlm.nih.gov/geo/query/acc.cgi?acc=GSE102105), which is composed of GSE102043 and GSE102104.

Supplementary Material

Refer to Web version on PubMed Central for supplementary material.

ACKNOWLEDGMENTS

We thank Lucia De Castro De Penaranda for helping in flight-test assays and M. Spletter for helpful discussions. We are grateful to A. Lalouette, R.M. Cripps, the Bloomington Drosophila (supported by NIH grant P40OD018537), the Vienna Drosophila Resource Center, and the TRiP at Harvard Medical School for fly stocks; to B. Paterson, the Babraham Institute, and the Developmental Studies Hybridoma Bank (DSHB) for antibodies; and to Flybase for online resources on the Database of Drosophila Genes & Genomes. We thank the Drosophila Genomics Resource Center (DGRC, supported by NIH grant 2P40OD010949-10A1) for cell lines and the Genomic Facility of the University of Chicago supported by Cancer Center Support Grant (P30 CA014599). This work was supported by NIH grants GM93827 and GM110018 (to M.V.F.) and by a postdoctoral fellowship from the American Heart Association (14POST20210010 to M.P.Z.).

REFERENCES

Acharya P, Raj N, Buckley MS, Zhang L, Duperon S, Williams G, Henry RW, and Arnosti DN (2010). Paradoxical instability-activity relationship defines a novel regulatory pathway for retinoblastoma proteins. Mol. Biol. Cell 21, 3890–3901. [PubMed: 20861300]

Althammer S, González-Vallinas J, Ballaré C, Beato M, and Eyras E (2011). Pyicos: a versatile toolkit for the analysis of high-throughput sequencing data. Bioinformatics 27, 3333–3340. [PubMed: 21994224]

Anders S, and Huber W (2010). Differential expression analysis for sequence count data. Genome Biol. 11, R106. [PubMed: 20979621]

Ashburner M, Ball CA, Blake JA, Botstein D, Butler H, Cherry JM, Davis AP, Dolinski K, Dwight SS, Eppig JT, et al.; The Gene Ontology Consortium (2000). Gene ontology: tool for the unification of biology. Nat. Genet 25, 25–29. [PubMed: 10802651]

Bailey TL, and Elkan C (1994). Fitting a Mixture Model by Expectation Maximization to Discover Motifs in Biopolymers (AAAI Press).

Benevolenskaya EV, Murray HL, Branton P, Young RA, and Kaelin WG, Jr. (2005). Binding of pRB to the PHD protein RBP2 promotes cellular differentiation. Mol. Cell 18, 623–635. [PubMed: 15949438]

Benjamini Y, and Hochberg Y (1995). Controlling the false discovery rate: a practical and powerful approach to multiple testing. J. R. Stat. Soc. B Stat. Methodol 57, 289–300.

Blanchet E, Annicotte J-S, Lagarrigue S, Aguilar V, Clapé C, Chavey C, Fritz V, Casas F, Apparailly F, Auwerx J, and Fajas L (2011). E2F transcription factor-1 regulates oxidative metabolism. Nat. Cell Biol 13, 1146–1152. [PubMed: 21841792]

Bryantsev AL, Baker PW, Lovato TL, Jaramillo MS, and Cripps RM (2012). Differential requirements for Myocyte Enhancer Factor-2 during adult myogenesis in Drosophila. Dev. Biol. 361, 191–207. [PubMed: 22008792]

Buttitta LA, Katzaroff AJ, Perez CL, de la Cruz A, and Edgar BA (2007). A double-assurance mechanism controls cell cycle exit upon terminal differentiation in Drosophila. Dev. Cell 12, 631–643. [PubMed: 17419999]

Classon M, Kennedy BK, Mulloy R, and Harlow E (2000). Opposing roles of pRB and p107 in adipocyte differentiation. Proc. Natl. Acad. Sci. USA 97, 10826–10831. [PubMed: 10995476]

de Bruin A, Wu L, Saavedra HI, Wilson P, Yang Y, Rosol TJ, Weinstein M, Robinson ML, and Leone G (2003). Rb function in extraembryonic lineages suppresses apoptosis in the CNS of Rb-deficient mice. Proc. Natl. Acad. Sci. USA 100, 6546–6551. [PubMed: 12732721]

Dimova DK, Stevaux O, Frolov MV, and Dyson NJ (2003). Cell cycle-dependent and cell cycle-independent control of transcription by the Drosophila E2F/RB pathway. Genes Dev. 17, 2308–2320. [PubMed: 12975318]

Du W, and Dyson N (1999). The role of RBF in the introduction of G1 regulation during Drosophila embryogenesis. EMBO J. 18, 916–925. [PubMed: 10022834]

Du W, Vidal M, Xie J-E, and Dyson N (1996). RBF, a novel RB-related gene that regulates E2F activity and interacts with cyclin E in Drosophila. Genes Dev. 10, 1206–1218. [PubMed: 8675008]

Dutta D, Anant S, Ruiz-Gomez M, Bate M, and VijayRaghavan K (2004). Founder myoblasts and fibre number during adult myogenesis in Drosophila. Development 131, 3761–3772. [PubMed: 15262890]

Dyson NJ (2016). RB1: a prototype tumor suppressor and an enigma. Genes Dev. 30, 1492–1502. [PubMed: 27401552]

Fernandes J, Bate M, and Vijayraghavan K 1991). Development of the indirect flight muscles of Drosophila. Development 113, 67–77. [PubMed: 1765009]

Firth LC, and Baker NE (2005). Extracellular signals responsible for spatially regulated proliferation in the differentiating Drosophila eye. Dev. Cell 8, 541–551. [PubMed: 15809036]

Georlette D, Ahn S, MacAlpine DM, Cheung E, Lewis PW, Beall EL, Bell SP, Speed T, Manak JR, and Botchan MR (2007). Genomic profiling and expression studies reveal both positive and negative activities for the Drosophila Myb MuvB/dREAM complex in proliferating cells. Genes Dev. 21, 2880–2896. [PubMed: 17978103]

Guarner A, Morris R, Korenjak M, Boukhali M, Zappia MP, Van Rechem C, Whetstine JR, Ramaswamy S, Zou L, Frolov MV, et al. (2017). E2F/DP Prevents Cell-Cycle Progression in Endocycling Fat Body Cells by Suppressing dATM Expression. Dev. Cell 43, 689–703.e5. [PubMed: 29233476]

Heinz S, Benner C, Spann N, Bertolino E, Lin YC, Laslo P, Cheng JX, Murre C, Singh H, and Glass CK (2010). Simple combinations of lineagedetermining transcription factors prime cis-regulatory elements required for macrophage and B cell identities. Mol. Cell 38, 576–589. [PubMed: 20513432]

Hirose F, Yamaguchi M, Handa H, Inomata Y, and Matsukage A (1993). Novel 8-base pair sequence (Drosophila DNA replication-related element) and specific binding factor involved in the

expression of Drosophila genes for DNA polymerase α and proliferating cell nuclear antigen. J. Biol. Chem 268, 2092–2099. [PubMed: 8093616]

Hubbard TJP, Aken BL, Beal K, Ballester B, Caccamo M, Chen Y, Clarke L, Coates G, Cunningham F, Cutts T, et al. (2007). Ensembl 2007. Nucleic Acids Res. 35, D610–D617. [PubMed: 17148474]

Korenjak M, Anderssen E, Ramaswamy S, Whetstine JR, and Dyson NJ (2012). RBF binding to both canonical E2F targets and noncanonical targets depends on functional dE2F/dDP complexes. Mol. Cell. Biol 32, 4375–4387. [PubMed: 22927638]

Korenjak M, Kwon E, Morris RT, Anderssen E, Amzallag A, Ramaswamy S, and Dyson NJ (2014). dREAM co-operates with insulator-binding proteins and regulates expression at divergently paired genes. Nucleic Acids Res. 42, 8939–8953. [PubMed: 25053843]

Langmead B, Trapnell C, Pop M, and Salzberg SL (2009). Ultrafast and memory-efficient alignment of short DNA sequences to the human genome. Genome Biol. 10, R25. [PubMed: 19261174]

Lewis PW, Beall EL, Fleischer TC, Georlette D, Link AJ, and Botchan MR (2004). Identification of a Drosophila Myb-E2F2/RBF transcriptional repressor complex. Genes Dev. 18, 2929–2940. [PubMed: 15545624]

Liao Y, Smyth GK, and Shi W (2013). The Subread aligner: fast, accurate and scalable read mapping by seed-and-vote. Nucleic Acids Res. 41, e108. [PubMed: 23558742]

Lilly B, Zhao B, Ranganayakulu G, Paterson BM, Schulz RA, and Olson EN (1995). Requirement of MADS domain transcription factor D-MEF2 for muscle formation in Drosophila. Science 267, 688–693. [PubMed: 7839146]

Liu YH, Jakobsen JS, Valentin G, Amarantos I, Gilmour DT, and Furlong EEM (2009). A systematic analysis of Tinman function reveals Eya and JAK-STAT signaling as essential regulators of muscle development. Dev. Cell 16, 280–291. [PubMed: 19217429]

McGuire SE, Mao Z, and Davis RL (2004). Spatiotemporal gene expression targeting with the TARGET and gene-switch systems in Drosophila. Sci. STKE 2004, pl6.

Nicolay BN, Gameiro PA, Tschöp K, Korenjak M, Heilmann AM, Asara JM, Stephanopoulos G, Iliopoulos O, and Dyson NJ (2013). Loss of RBF1 changes glutamine catabolism. Genes Dev. 27, 182–196. [PubMed: 23322302]

Novitch BG, Spicer DB, Kim PS, Cheung WL, and Lassar AB (1999). pRb is required for MEF2-dependent gene expression as well as cell-cycle arrest during skeletal muscle differentiation. Curr. Biol 9, 449–459. [PubMed: 10322110]

Perez-Llamas C, and Lopez-Bigas N (2011). Gitools: analysis and visualisation of genomic data using interactive heat-maps. PLoS ONE 6, e19541. [PubMed: 21602921]

Petrov PD, Ribot J, López-Mejía IC, Fajas L, Palou A, and Bonet ML (2016). Retinoblastoma Protein Knockdown Favors Oxidative Metabolism and Glucose and Fatty Acid Disposal in Muscle Cells. J. Cell. Physiol 231, 708–718. [PubMed: 26241807]

Quinlan AR, and Hall IM (2010). BEDTools: a flexible suite of utilities for comparing genomic features. Bioinformatics 26, 841–842. [PubMed: 20110278]

Reedy MC, and Beall C (1993). Ultrastucture of developing flight muscle in Drosophila, I: Assembly of Myofibrils. Dev. Biol 160, 443–465. [PubMed: 8253277]

Robinson JT, Thorvaldsdóttir H, Winckler W, Guttman M, Lander ES, Getz G, and Mesirov JP (2011). Integrative genomics viewer. Nat. Biotechnol 29, 24–26. [PubMed: 21221095]

Schneider JW, Gu W, Zhu L, Mahdavi V, and Nadal-Ginard B (1994). Reversal of terminal differentiation mediated by p107 in Rb−/− muscle cells. Science 264, 1467–1471. [PubMed: 8197461]

Schnorrer F, Schönbauer C, Langer CCH, Dietzl G, Novatchkova M, Schernhuber K, Fellner M, Azaryan A, Radolf M, Stark A, et al. (2010). Systematic genetic analysis of muscle morphogenesis and function in Drosophila. Nature 464, 287–291. [PubMed: 20220848]

Schones DE, Smith AD, and Zhang MQ (2007). Statistical significance of cis-regulatory modules. BMC Bioinformatics 8, 19. [PubMed: 17241466]

Shannon P, Markiel A, Ozier O, Baliga NS, Wang JT, Ramage D, Amin N, Schwikowski B, and Ideker T (2003). Cytoscape: a software environment for integrated models of biomolecular interaction networks. Genome Res. 13, 2498–2504. [PubMed: 14597658]

Shin H, Liu T, Manrai AK, and Liu XS (2009). CEAS: cis-regulatory element annotation system. Bioinformatics 25, 2605–2606. [PubMed: 19689956]

Soler C, Han J, and Taylor MV (2012). The conserved transcription factor Mef2 has multiple roles in adult Drosophila musculature formation. Development 139, 1270–1275. [PubMed: 22357930]

Sparrow JC, and Schöck F (2009). The initial steps of myofibril assembly: integrins pave the way. Nat. Rev. Mol. Cell Biol 10, 293–298. [PubMed: 19190670]

Spike BT, Dirlam A, Dibling BC, Marvin J, Williams BO, Jacks T, and Macleod KF (2004). The Rb tumor suppressor is required for stress erythropoiesis. EMBO J. 23, 4319–4329. [PubMed: 15457215]

Spletter ML, Barz C, Yeroslaviz A, Schönbauer C, Ferreira IRS, Sarov M, Gerlach D, Stark A, Habermann BH, and Schnorrer F (2015). The RNA-binding protein Arrest (Bruno) regulates alternative splicing to enable myofibril maturation in Drosophila flight muscle. EMBO Rep. 16, 178–191. [PubMed: 25532219]

Spletter ML, Barz C, Yeroslaviz A, Zhang X, Lemke SB, Bonnard A, Brunner E, Cardone G, Basler K, Habermann BH, and Schnorrer F (2018). A transcriptomics resource reveals a transcriptional transition during ordered sarcomere morphogenesis in flight muscle. eLife 7, e34058. [PubMed: 29846170]

Sturn A, Quackenbush J, and Trajanoski Z (2002). Genesis: cluster analysis of microarray data. Bioinformatics 18, 207–208. [PubMed: 11836235]

Sudarsan V, Anant S, Guptan P, VijayRaghavan K, and Skaer H (2001). Myoblast diversification and ectodermal signaling in Drosophila. Dev. Cell 1, 829–839. [PubMed: 11740944]

Tansey T, Schultz JR, Miller RC, and Storti RV (1991). Small differences in Drosophila tropomyosin expression have significant effects on muscle function. Mol. Cell. Biol 11, 6337–6342. [PubMed: 1719381]

Thomas DM, Carty SA, Piscopo DM, Lee JS, Wang WF, Forrester WC, and Hinds PW (2001). The retinoblastoma protein acts as a transcriptional coactivator required for osteogenic differentiation. Mol. Cell 8,303–316. [PubMed: 11545733]

Trapnell C, Pachter L, and Salzberg SL (2009). TopHat: discovering splice junctions with RNA-Seq. Bioinformatics 25, 1105–1111. [PubMed: 19289445]

Ui K, Ueda R, and Miyake T (1987). Cell lines from imaginal discs of Drosophila melanogaster. In Vitro Cell Dev. Biol 23, 707–711. [PubMed: 3117765]

Váraljai R, Islam ABMMK, Beshiri ML, Rehman J, Lopez-Bigas N, and Benevolenskaya EV (2015). Increased mitochondrial function downstream from KDM5A histone demethylase rescues differentiation in pRB-deficient cells. Genes Dev. 29, 1817–1834. [PubMed: 26314709]

Weitkunat M, and Schnorrer F (2014). A guide to study Drosophila muscle biology. Methods 68, 2–14. [PubMed: 24625467]

Weitkunat M, Kaya-Çopur A, Grill SW, and Schnorrer F (2014). Tension and force-resistant attachment are essential for myofibrillogenesis in Drosophila flight muscle. Curr. Biol 24, 705–716. [PubMed: 24631244]

Zacksenhaus E, Jiang Z, Chung D, Marth JD, Phillips RA, and Gallie BL (1996). pRb controls proliferation, differentiation, and death of skeletal muscle cells and other lineages during embryogenesis. Genes Dev. 10, 3051–3064. [PubMed: 8957005]

Zappia MP, and Frolov MV (2016). E2F function in muscle growth is necessary and sufficient for viability in Drosophila. Nat. Commun 7, 10509. [PubMed: 26823289]

Zhang Y, Liu T, Meyer CA, Eeckhoute J, Johnson DS, Bernstein BE, Nusbaum C, Myers RM, Brown M, Li W, and Liu XS (2008). Modelbased analysis of ChIP-Seq (MACS). Genome Biol. 9, R137. [PubMed: 18798982]

Highlights

- The tumor suppressor Rbf promotes muscle growth and myofibrillogenesis
- The loss of Rbf severely affects the myogenic transcriptic program
- Rbf activates the transcription of myogenic genes in an E2F dependent manner
- Rbf genetically interacts with usp, ct, and Stat92E in late myogenesis

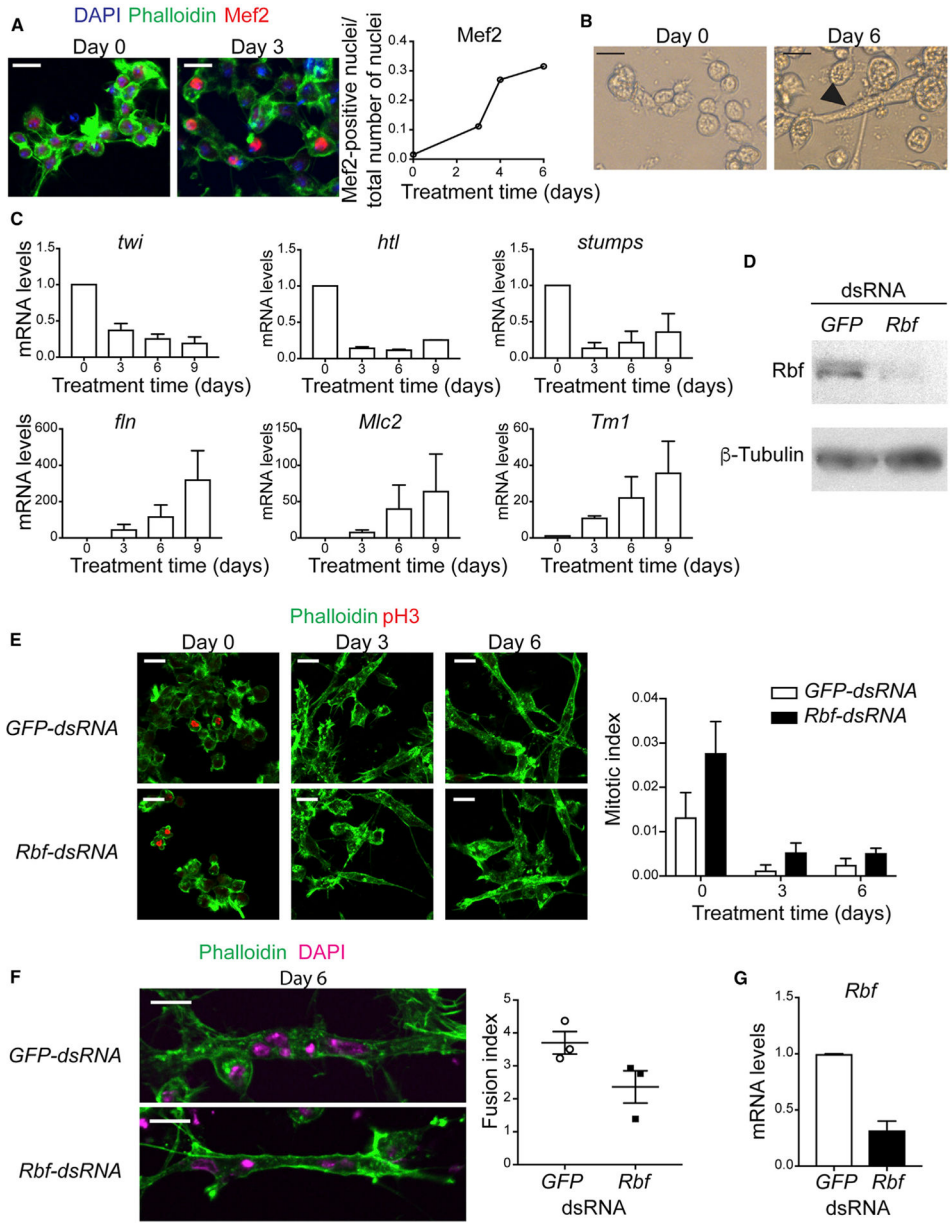

Figure 1. The Function of Rbf Is Required to Differentiate Dmd8 Cells into Myotubes

(A) Dmd8 myoblasts were treated with differentiation medium for 0, 2, 4, and 6 days and stained with anti-Mef2 antibody, phalloidin and DAPI. Confocal images at day 0 and 3. Quantification of the number of Mef2-positive nuclei normalized to the number of nuclei. Mean. Experiment was done at least twice with n = 10 images with 80–400 cells per image.

(B) Brightfield image of elongated myotube at day 6 after treatment.

(C) mRNA expression level of the genes *twist (twi), heartless (htl), stumps, flightin (fln), Myosin light chain 2* (*Mlc2*), and *Tropomyosin 1 (Tm1-H)* at day 0,3,6, and 9 after treatment. Mean ± SEM, n = 2.

(D) Lysates of Dmd8 cells treated for 4 days with *GFP-dsRNA* and *Rbf-dsRNA*, blotted against Rbf and β-tubulin.

(E) Confocal images of Dmd8 cells treated with *GFP*-dsRNA and *Rbf*-dsRNA at day 0, 3, and 6, stained with phalloidin and anti-pH3. Quantification of the number of pH3-positive nuclei normalized to number of nuclei. Mean ± SEM, experiment was done three times once with n = 6 images and twice with n = 10 images with 100–400 cells per image, two-way ANOVA, $p > 0.05$.

(F) Confocal images of Dmd8 cells treated with *GFP*-dsRNA and *Rbf*-dsRNA at day 6, stained with phalloidin and DAPI. Quantification of the number of nuclei per myotube. Mean ± SEM, experiment was done three times with n = 10 images with between 2 and 6 myotubes per image, Mann-Whitney test, $p > 0.05$.

(G) mRNA expression levels of *Rbf* at day 6 after treatment. Mean ± SEM, n = 2. Mann-Whitney test, $p > 0.05$.

Scale bar (A, B, E, F), 10 μm.

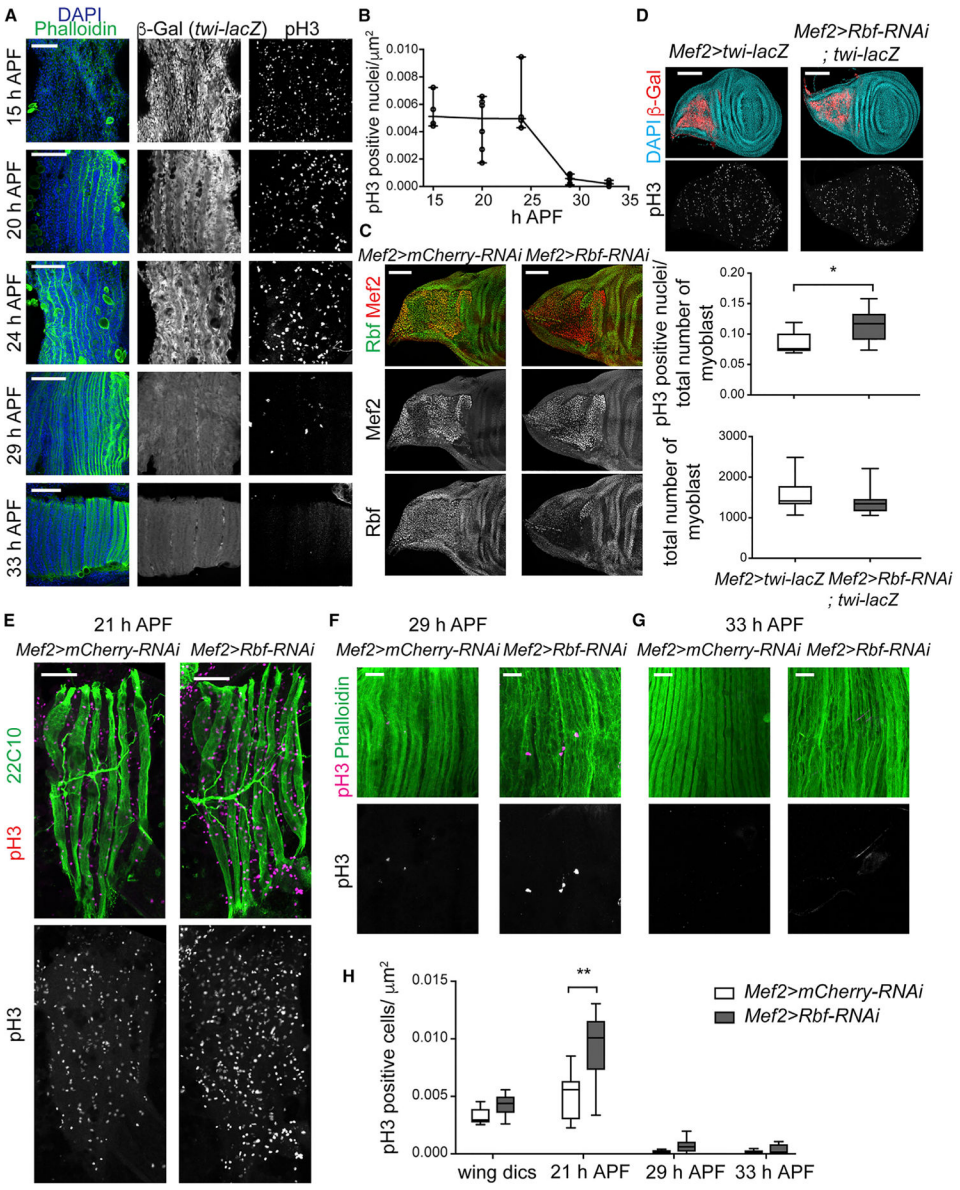

Figure 2. The Loss of Rbf Impairs Cell Cycle Progression in Proliferating Myoblasts before Fusion

(A and B) Developing DLMs stained over time from 15 to 33 h APF with phalloidin and DAPI, *twi-lacZ* reporter, and anti-pH3 antibody.

(A) Single confocal sections for phalloidin, DAPI, and *twi-lacZ* reporter expect for pH3 staining, which are maximum projections of z-stacks.

(B) Number of pH3-positive nuclei relative to DLM area. Scatterplot, n = 4–6 animals/time point.

(C) Confocal sections of wing discs of third-instar larvae stained using anti-Rbf and Mef2-antibodies.

(D) Confocal images of wing discs of third-instar larvae stained with anti-pH3, *twi-lacZ* reporter (anti-β-Gal antibody), and DAPI. Maximum projections of z-stacks. Quantification of both pH3-positive nuclei relative to total number of myoblast and the total number of

myoblasts. Box plot (median and quartiles), whiskers (minimum to maximum), Mann-Whitney test, *p < 0.05, two-tailed, n = 9-10 discs/genotype.

(E–G) Developing DLMs at 21 h APF (E), 29 h APF (F), and 33 h APF (G) labeled with anti-pH3 (magenta), and the marker 22c10 (E) or phalloidin (F and G). Single confocal sections (E) and maximum projection of *z*-stack from confocal images (F and G).

(H) Quantification of number of pH3-positive nuclei relative to DLM area. Box plot (median and quartiles), whiskers (minimum to maximum), two-way ANOVA followed by Bonferroni's multiple comparisons test, **p < 0.01, n = 6–10 animals/genotype and time point.

Full genotypes are (A) *w-; twi-lacZ; Mef2-GAL4,* (C, E, F, and G) *w-, UAS-Dicer2; +; Mef2-GAL4/UAS-mCherry-RNAi* and *w-, UAS-Dicer2; +; Mef2-GAL4/UAS-Rbf-RNAi,* (D) *w-, UAS-Dicer2; twi-lacZ; Mef2-GAL4* and *w-, UAS-Dicer2; twi-lacZ; Mef2-GAL4/UAS-Rbf-RNAi.* Scale bars, 50 μm (A and E), 100 μm (C and D), and 20 μm (F and G). See also Figure S1.

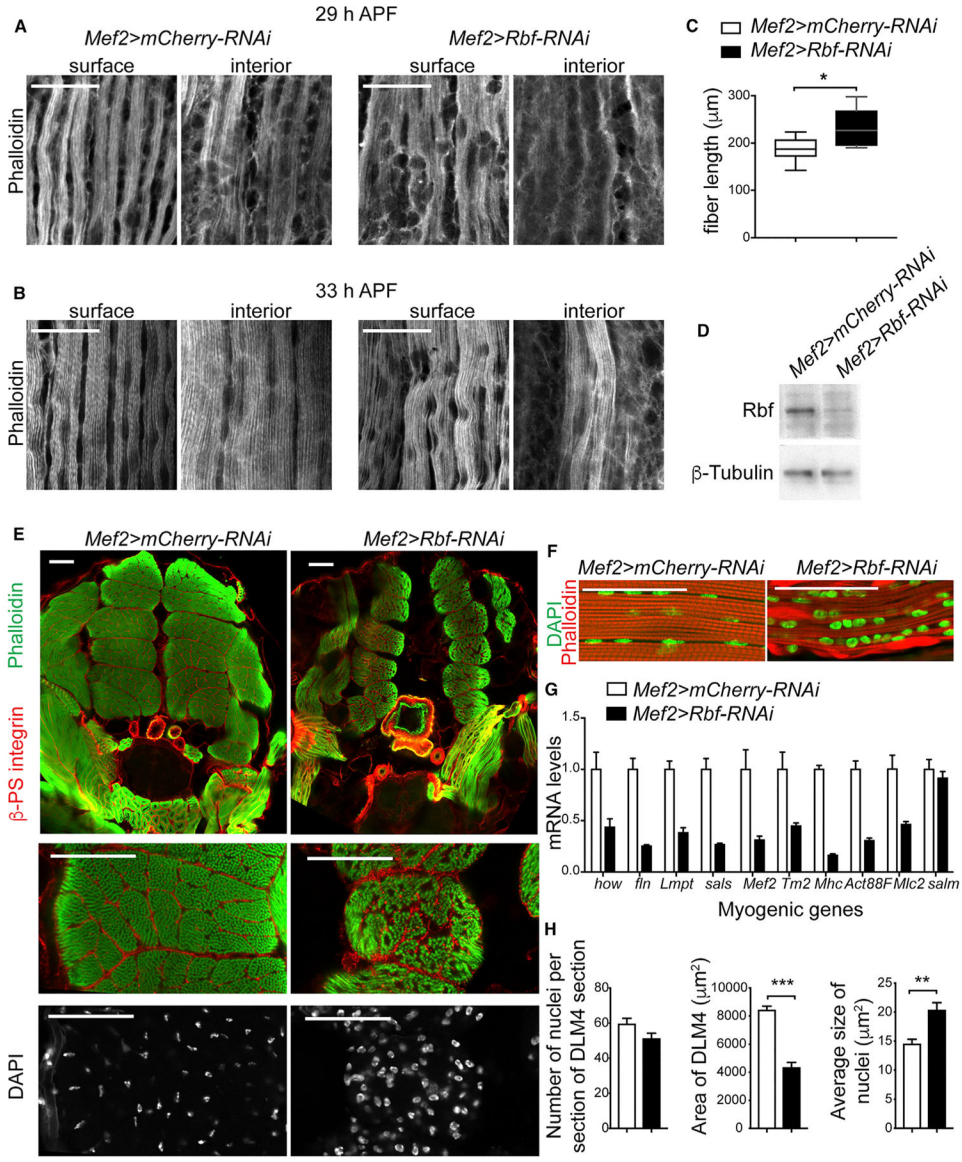

Figure 3. The Loss of Rbf Impairs Myofibrillogenesis and Muscle Growth

(A and B) Two confocal section images of developing DLMs stained using phalloidin at 29 h APF (A) and 33 h APF (B). Interior plane was taken 4 μm below the surface plane.

(C) Length of DLM at 29 h APF. Box plot (median), whisker (5–95 percentile), Mann-Whitney, two-tailed, *p < 0 0.05, n = 10 animals.

(D) Lysates of thoracic muscles at 96 h APF blotted against Rbf and β-tubulin antibodies.

(E)Confocal section images of transverse sections of thoraces at 96 h APF stained using anti-β-PS-integrin antibody, phalloidin, and DAPI, ventral to bottom. Magnification of DLM4 is at the bottom.

(F) Confocal section images of sagittal sections of thoraces at 96 h APF stained with phalloidin and DAPI, ventral to bottom.

(G) mRNA expression levels ofthegenes *held out wings* (*how*), *flightin (fln), Limpet* (*Lmpt*-K), *sarcomere length short* (*sals*), *Mef2, Tropomyosin2* (*Tm2*), *Myosin heavy chain* (*Mhc*),

Actin88F(Act88F), Myosin light chain 2 (*Mlc2*), and *spalt major (salm)* measured in thoracic muscles at 96 h APF. Mean ± SEM, n = 3 samples/genotype.

(H) The number of nuclei, the area, and the average size of nuclei in DLM4 transverse sections of thoraces at 96 h APF quantified/animal. Mean ± SEM, Mann-Whitney, two-tailed, **p < 0 0.01, ***p < 0 0.001, n = 9 animals/genotype.

Full genotypes are *w-, UAS-Dicer2; +; Mef2-GAL4/UAS-mCherry-RNAi and w-, UAS-Dicer2; +; Mef2-GAL4/UAS-Rbf-RNAi*. Scale bars, 20 μm (A and B) and 50 μm (E and F).

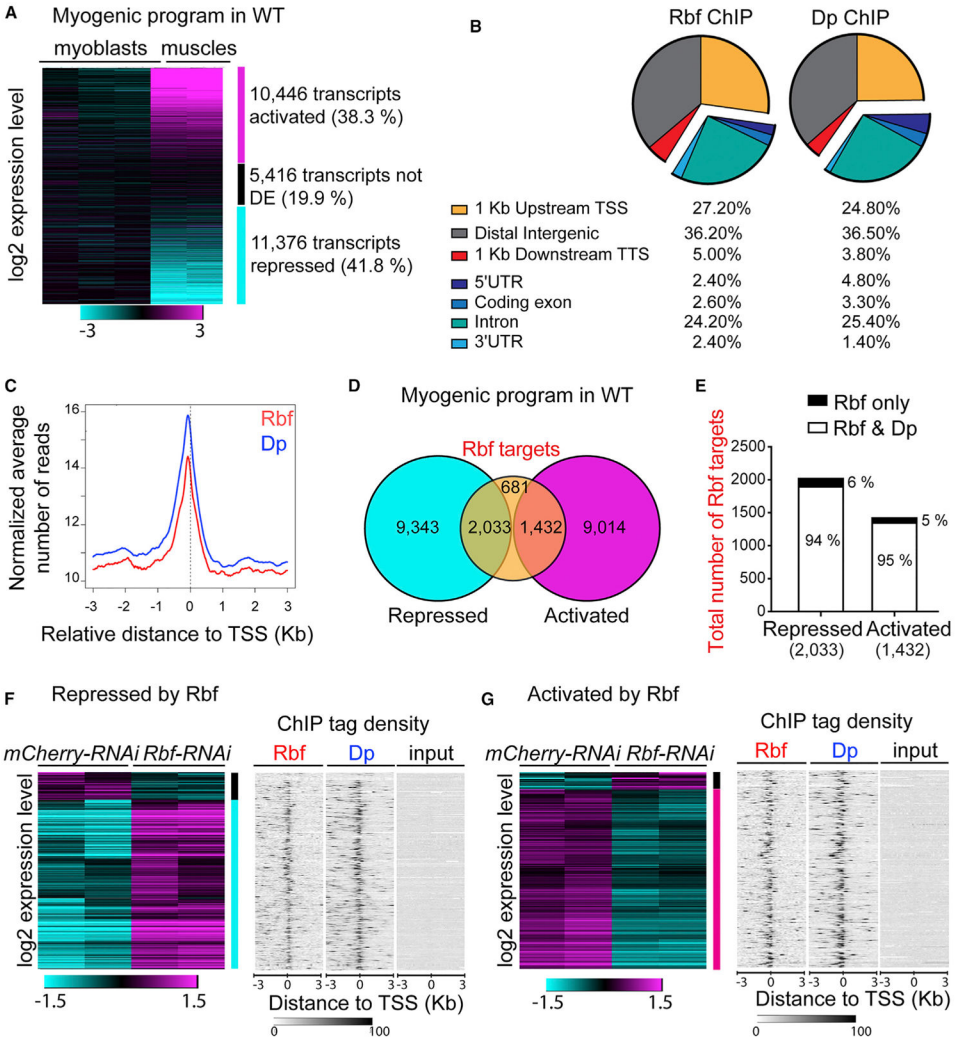

Figure 4. Rbf Activates the Myogenic Transcriptional Program

(A) Heat map representing $\log_2$-fold change expression levels of transcripts in the flight muscles at 96 h APF relative to the notum of the third-instar larvae in wild-type animals using Genesis. Total of 27,238 transcripts (muscles versus myoblasts). n = 3 samples of wing disc notums; n = 2 samples of mature muscles.

(B) Genomic occupancy profile of Rbf and Dp in flight muscles of wild-type animals at 96 h APF annotated using Cis-Regulatory Element Annotation System (CEAS); 4,146 transcripts defined as Rbf targets, n = 2 independent samples per antibody and two input samples.

(C) Average profile of Rbf (red, 3,470 peaks) and Dp (blue, 5,148 peaks) mapped reads in 50 bp plotted near the TSS in kilobase using CEAS.

(D) Overlap between Rbf-direct targets (4,146 transcripts) and transcripts that are either repressed (11,376 transcripts) or activated (10,446 transcripts) during myogenic program in wild type (WT; muscles versus myoblasts).

(E) Among the 2,033 transcripts that are both Rbf targets and repressed in WT, 1,906 transcripts are also Dp targets (94%) and 127 are not (6%). Among the 1,432 transcripts that

are both Rbf targets and activated in WT, 1,358 are also Dp targets (95%) and 74 are not (5%).

(F) Number of Rbf targets that are repressed in WT but are differentially expressed in *Mef2>Rbf-RNAi* muscles compared with *Mef2>mCherry-RNAi*; 160 transcripts are downregulated (black vertical bar) and 986 transcripts are upregulated (cyan vertical bar, defined as transcripts repressed by Rbf).

(G) Rbf targets that are activated in WT but differentially expressed in *Mef2>Rbf-RNAi* muscles compared with *Mef2>mCherry-RNAi* muscles; 81 transcripts are upregulated and 851 transcripts downregulated (magenta vertical bar, defined as transcripts activated by Rbf).

(F and G) Left: Heat map representing $\log_2$-fold change expression levels of transcripts in the flight muscles at 96 h APF in *Mef2>Rbf-RNAi* relative to *Mef2>mCherry-RNAi* animals using hierarchical clustering, Pearson correlation distance in Genesis n = 2 samples/genotype. Right: Sequence tag-density heat map for Rbf and Dp distribution peaks near the TSS of transcripts compared with input sample. n = 2 samples/condition. Gitools was used. Full genotypes are (A, F, and G) *w-, UAS-Dicer2; +; Mef2-GAL4/UAS-mCherry-RNAi*, and (F and G) *w-, UAS-Dicer2; +; Mef2-GAL4/UAS-Rbf-RNAi*.

See also Table S1, S2, S3, and S4.

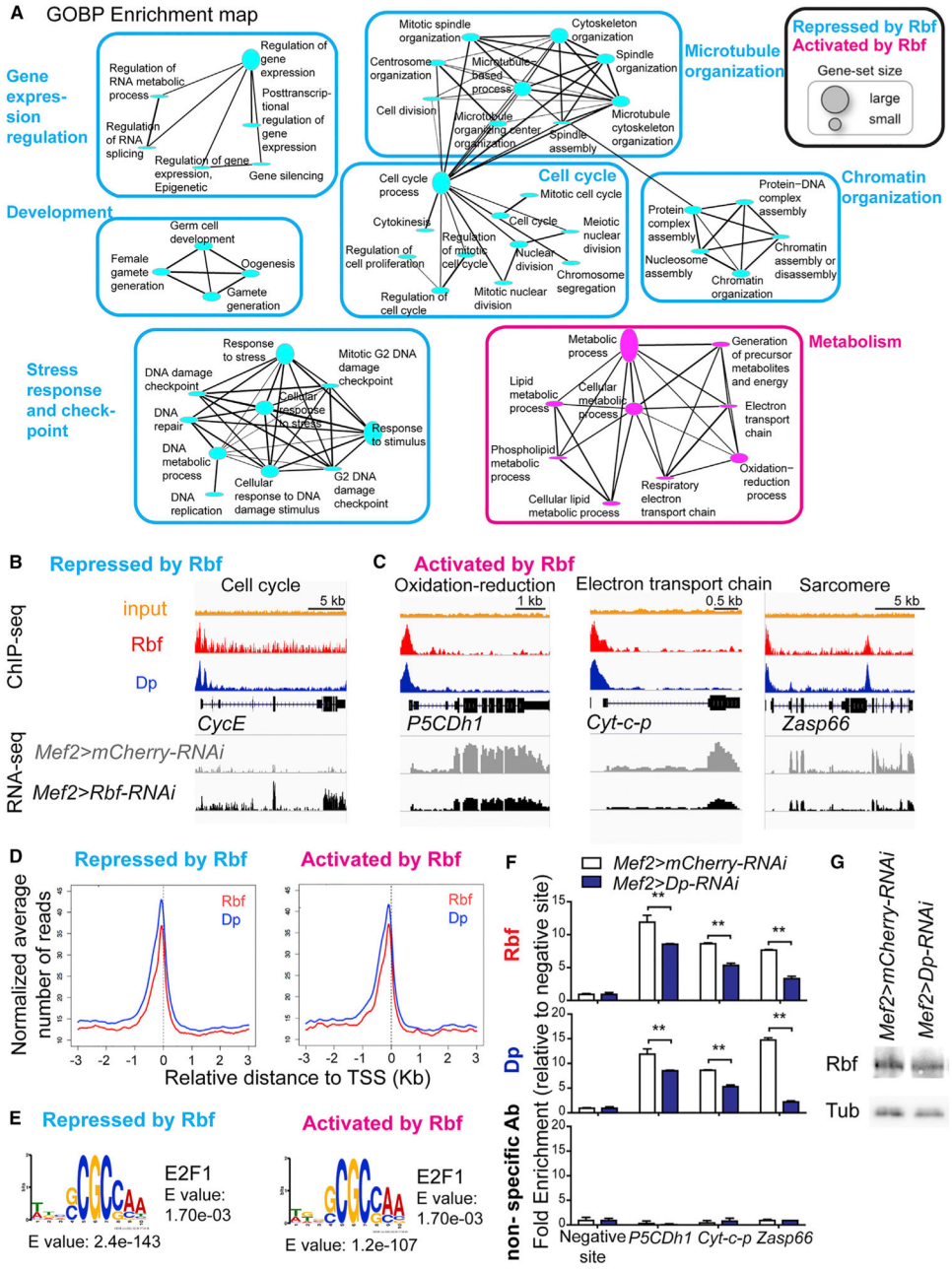

Figure 5. Rbf Activates the Expression of Metabolic Genes in Muscle

(A) Functional biological processes directly repressed (986 transcripts) and activated (851 transcripts) by Rbf in muscles. GO terms visualized as an enrichment map, clustered using Cytoscape. Size of gene-set is scaled based on the number of genes enriched.

(B and C) ChIP-Seq and RNA-Seq data visualized with Integrative Genomics Viewer browser for the genomic regions surrounding the genes (B) *Cyclin E (CycE),* (C) *delta-1-Pyrroline-5-carboxylate dehydrogenase 1 (P5CDh1), Cytochrome c proximal* (*Cyt-c-p*), and *Z band alternatively spliced PDZ-motif protein 66* (*Zasp66*). n = 2 samples/condition. The expression of these genes in *Mef2>mCherry-RNAi* muscles and *Mef2>Rbf-RNAi* in muscles is displayed with the reads assembled. n = 2/genotype. Read scales are (B) 0–15 in

Rbf ChIP, 0–92 in Dp ChIP, and 0–44 in RNA-seq for *CycE*; (C) 0–29, 0–109, and 0–296 for *P5CDh1;* 0–33, 0–123, and 0–869 for *Cyt-c-p;* and 0–23, 0–85, and 0–381 for *Zasp66,* respectively. GroupAuto scale was used for RNA-seq.

(D) Average profile of Rbf (red) and Dp (blue) mapped reads in 50 bp plotted near the TSS in kilobase using Cis-Regulatory Element Annotation System (CEAS) for sequences repressed by Rbf (986 transcripts) and activated by Rbf (851 transcripts).

(E) *De novo* motif discovery MEME. Sequences repressed by Rbf (986 transcripts and 575 peaks) and activated by Rbf (851 transcripts and 404 peaks). TOMTOM matched the motif against the vertebrate database.

(F) ChIP-qPCR from pupae (96 h APF) using anti-Rbf, anti-Dp, and nonspecific antibodies (IgG and anti-Myc). Genes are *P5CDh1, Cyt-c-p,* and *Zasp66.* Fold-enrichment relative to the negative site for each ChIP sample. Mean ± SD, n = 2 replicates per antibody, two-way ANOVA, Bonferroni's multiple comparisons test, $^{**}p < 0.01$.

(G) Lysates of pupae (96 h APF) blotted against Rbf and β-tubulin antibodies. Genotypes are *Mef2-GAL4/UAS-mCherry-RNAi* and *UAS-Dp-RNAi;Mef2-GAL4.* See also Table S5.

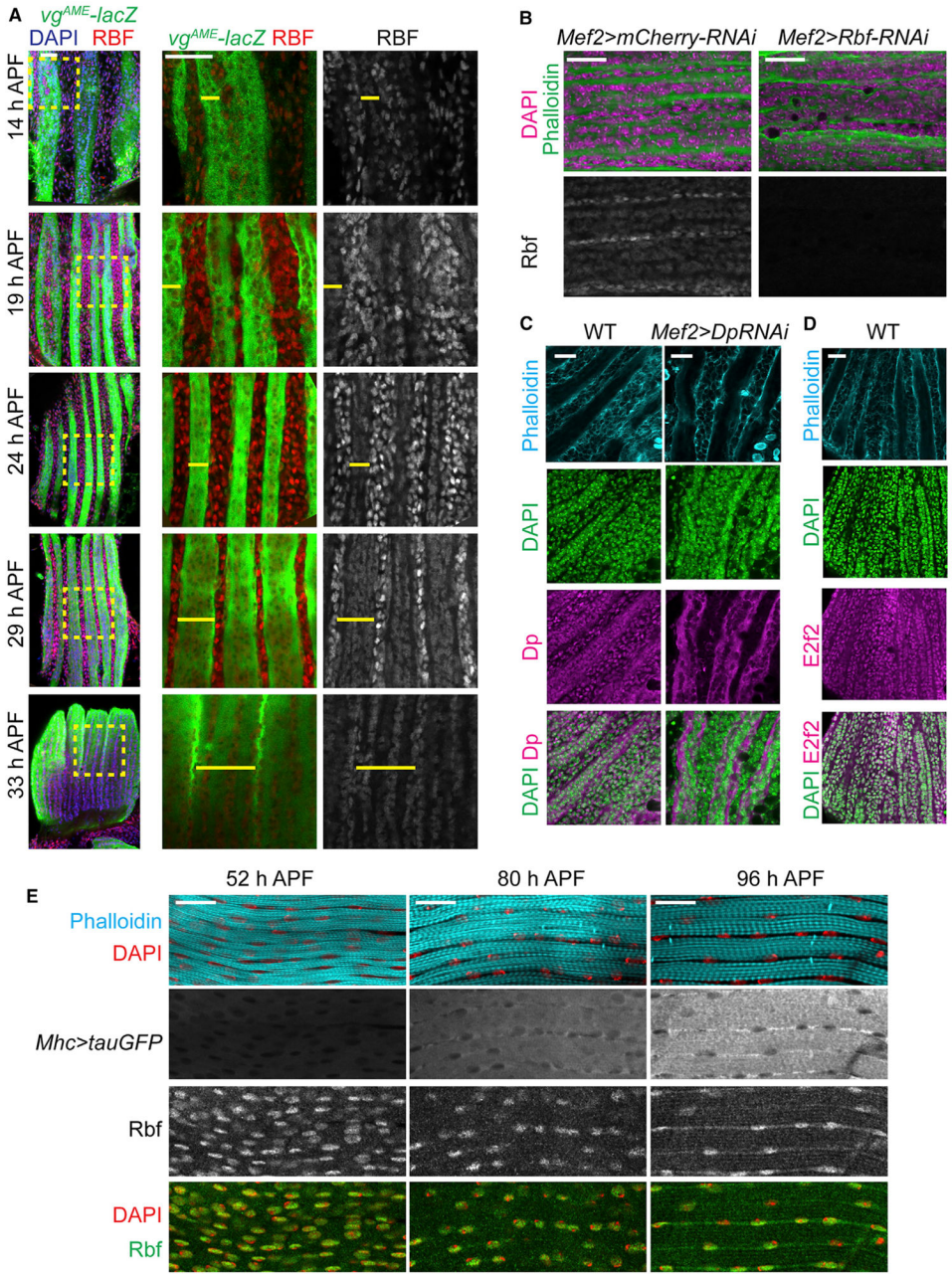

Figure 6. The Expression Level of Rbf Switched from Proliferating Myoblasts to Developing Myotubes

(A) Developing DLMs labeled using *vgAME-lacZ* reporter (yellow bar) and anti-Rbf antibodies from 14 to 33 h APF. Magnified images of the yellow, dashed boxes indicated on the overlay image on the left.

(B) Developing DLMs at 29 h APF stained with anti-Rbf antibody, phalloidin, and DAPI in *Mef2>mCherry-RNAi* and *Mef2>Rbf-RNAi* as negative control.

(C and D) Developing DLMs staged at 24 h APF (C) and 21 h APF (D) stained with phalloidin, DAPI, anti-Dp (C) and anti-E2f2 (D) antibodies. *Mef2>Dp-RNAi* was used as negative control.

(E) Developing DLMs labeled using *Mhc>tauGFP,* anti-Rbf antibody, phalloidin, and DAPI from 52 to 96 h APF.

Genotypes are (A) *w-;vgAME-lacZ,* (B) *w-, UAS-Dicer2; +; Mef2-GAL4/UAS-mCherry-RNAi*, and *w-, UAS-Dicer2; +; Mef2-GAL4/UAS-Rbf-RNAi*, (C) *w-;vgAME-lacZ* as WT and *w-; UAS-Dp-RNAi; Mef2-GAL4,* (D) *y-w-,* and (E) *w-; P{Mhc-tauGFP}2*. Scale bars, 20 μm.

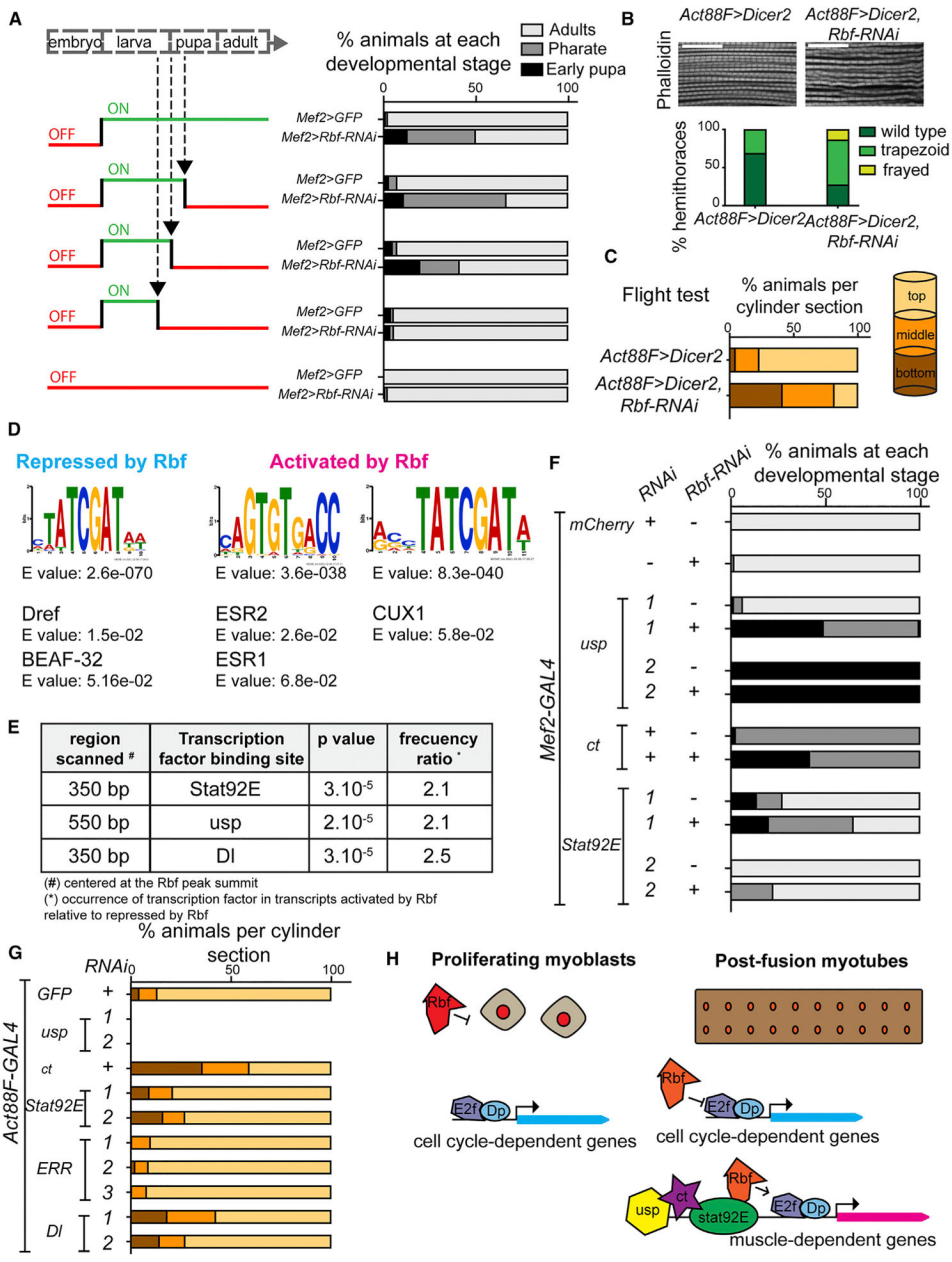

Figure 7. Rbf Affects the Maturation of Flight Muscles in Late Development and Interacts with Other Transcription Factors

(A) Rbf depletion in muscles was temporally induced with *tub-GAL80^{TS}* by switching ON the system at 31 °C to inactivate GAL80^{TS} and OFF (18°C) at midpupa development, early pupa development, and late third-instar larva. Percentage of animals scored at each developmental stage, n = 52–130 flies/genotype. Genotypes are *w-, tub-GAL80^{TS}/UAS-GFP; Mef2-GAL4,* and *w-, tub-GAL80^{TS}/UAS-Dicer2; Mef2-GAL4/UAS-Rbf1-RNAi.*

(B) Rbf depleted using *Act88F-GAL4* in flight muscles at late-pupa development. Confocal sections of sagittal sections of adult thoraces stained with phalloidin. Scale bar, 20 μm. Myofibril morphology quantified by scoring percentage of thoraces displaying phenotype. n = 16 and 22 hemithoraces/genotype.

(C) Flight ability scored as percentage of flies landing on each section of the column. n = 80 and 110 flies/genotype. Genotypes are *w-, Act88F-GAL4; UAS-Dicer2,* and *w-, Act88F-GAL4; UAS-Dicer2; UAS-Rbf1-RNAi.*

(D) *Denovo* motif discovery MEME. Sequences repressed by Rbf (986 transcripts and 575 peaks) and activated by Rbf (851 transcripts and 404 peaks). TOMTOM matched the motif against *Drosophila* (left) and vertebrate (right) databases.

(E) STORM-scanned sequences near Rbf peak in the two groups of transcripts (repressed and activated by Rbf).

(F) Genetic interactions between Rbf and the transcription factors, ultraspiracle (usp), cut (ct), and Signal-transducer and activator of transcription protein at 92E (Stat92E). Knockdown of each gene was driven by *Mef2-GAL4.* Lethality during development was scored as in (A). n = 140–474 flies/genotype.

(G) Flight test as in (C). n = 180–505 flies/genotype. Genotypes are (F) *Mef2-GAL4/UAS-mCherry-RNAi*, *UAS-Rbf-RNAi/Mef2-GAL4*, (G) *Act88F-GAL4;UAS-EGFP-RNAi*, (F and G) 1: *UAS-usp-RNAi*^{GD1554} and 2: *UAS-usp-RNAi*^{JF02546}, *UAS-ct-RNA*^{GD1237}, 1:*UAS-Stat92E-RNAi*^{HMS00035} and 2: *UAS-Stat92E-RNAi*^{JF01265}, (G) 1: *UAS-ERR-RNAi*^{HMJ23520}, 2: *UAS-ERR-RNAi*^{JF02431}, and 3: *UAS-ERR-RNAi*^{HMC03087}, 1: *UAS-Dl-RNAi*^{GD1238} and 2: *UAS-Dl-RNAi*^{JF02825}.

(H) Model representing how Rbf regulates flight muscle development *in vivo*. Canonical function of Rbf during myoblasts proliferation (left). Rbf restrains the activity of E2F in promoter of cell cycle genes. Role of Rbf as an activator of flight muscle development (right). Rbf directly activates and represses the expression of genes in growing muscles, which is mediated by E2F and other transcription factors, including usp, ct, and Stat92E. See also Table S6 and Figure S2.

KEY RESOURCES TABLE

REAGENT or RESOURCE	SOURCE	IDENTIFIER
Antibodies		
mouse anti-RBF (IF)	Du et al., 1996	DX2
mouse anti-RBF (WB)	Du et al., 1996	DX3
mouse anti-RBF (ChIP)	Du et al., 1996	DX3:DX5
rabbit anti-DP	Dimova et al., 2003	212
rabbit anti-pH3	Millipore	06-570
mouse anti-β-PS-integrin	DSHB	*CF*.6G11; RRID:AB_528310
mouse anti-futsch	DSHB	22c10; RRID:AB_528403
mouse anti-β-tubulin	DSHB	E7; RRID:AB_528499
mouse anti-β-Gal	DSHB	40-1a; RRID:AB_528100
rabbit anti-Mef2	Lilly et al., 1995	N/A
Critical Commercial Assays		
SensiFast SYBR No-ROX Mix	Bioline	BIO-98020
SensiFAST cDNA Synthesis Kit	Bioline	BIO-65053
Deposited Data		
Rbf and Dp ChIP-seq in muscles	This paper	GEO: GSE102043
RNA-seq of muscles and notum in wild type and Me2 > Rbf-RNAi	This paper	GEO: GSE102104
Drosophila EnsEMBL Biomart version 77, BDGP5.77	EnsEMBL (Hubbard et al., 2007)	N/A
Database of known motifs Eurakyote DNA (Vertebrates *in vivo* and *in silico*) and FLY DNA	Tomtom	http://meme-suite.org/tools/tomtom
Transfac database, insect metrix (professional version release 2009.4)	Transfac	N/A
Experimental Models: Cell Lines		
Drosophila melanogaster cell line: ML-Dmd8	DGRC	Flybase: FBtc0000092; RRID:CVCL_Z754
Experimental Models: Organisms/Strains		
Act88F-GAL4	Richard. M. Cripps	Bryantsev et al., 2012
P{twi- bgal}	Richard. M. Cripps	N/A
vgAME-lacZ	Alexis Lalouette	N/A
P{GAL4-Mef2.R}3	Bloomington Drosophila Stock Center	Flybase: FBst0027390
UAS-Rbf-RNAi	Vienna Drosophila Resource Center	Flybase: FBst0450139
UAS-Dp-RNAi	Vienna Drosophila Resource Center	Flybase: FBst0450633
P{VALIUM20-mCherry}attP2	Bloomington Drosophila Stock Center	Flybase: FBti0143385
P{tubP-GAL80[ts]}20	Bloomington Drosophila Stock Center	Flybase: FBti0027796
UAS-usp-RNAi^{GD1554}	Vienna Drosophila Resource Center	Flybase: FBst0452461
UAS-usp-RNAi^{JF02546}	Bloomington Drosophila Stock Center	Flybase: FBst0027258

REAGENT or RESOURCE	SOURCE	IDENTIFIER
UAS-ct-RNAi^{GD1237}	Vienna Drosophila Resource Center	Flybase: FBst0470085
UAS-Stat92E-RNAi^{HMS00035}	Bloomington Drosophila Stock Center	Flybase: FBst0033637
UAS-Stat92E-RNAi^{JF01265}	Bloomington Drosophila Stock Center	Flybase: FBst0031317
P{UAS-Dcr-2.D}1, w1118; P{GAL4-Mef2.R}R1	Bloomington Drosophila Stock Center	Flybase: FBst0025756
Oligonucleotides		
Primer sequence	This paper	Table S7
Software and Algorithms		
TopHat version 2.1.1	Trapnell et al., 2009	N/A
DESeq2 version 1.14.1 with R version 3.3.2 (2016-10-31)	Anders and Huber, 2010	N/A
BOWTIE version 2.3.2	Langmead et al., 2009	N/A
MACS version 1.4.2	Zhang et al., 2008	N/A
CEAS	Shin et al., 2009	http://liulab.dfci.harvard.edu/CEAS/
Integrative Genomics Viewer (IGV_2.3.79)	Robinson et al., 2011	http://software.broadinstitute.org/software/igv/
MEME	Bailey and Elkan, 1994	http://meme-suite.org/tools/meme
Cytoscape v3.3.0	Shannon et al., 2003	https://cytoscape.org
STORM	Schones et al., 2007	N/A
ImageJ 1.48v	NIH, USA	https://imagej.nih.gov/ij/download.html